

1 **Minimal cobalt metabolism in the marine cyanobacterium *Prochlorococcus***

2
3 Nicholas J. Hawco^{1,2,†,*}, Matthew M. McIlvin¹, Randelle M. Bundy^{1,3}, Alessandro Tagliabue⁴,
4 Tyler J. Goepfert^{1,5}, Dawn M. Moran¹, Luis Valentin-Alvarado^{1,6}, Giacomo R. DiTullio⁷ and
5 Mak A. Saito^{1*}

6
7 ¹ Department of Marine Chemistry and Geochemistry, Woods Hole Oceanographic Institution,
8 Woods Hole MA, USA

9 ² Department of Earth Sciences, University of Southern California, Los Angeles CA, USA

10 ³ School of Oceanography, University of Washington, Seattle WA, USA

11 ⁴ Department of Earth, Ocean and Ecological Sciences, University of Liverpool, Liverpool UK

12 ⁵ School of Earth and Space Exploration, Arizona State University, Tempe AZ, USA

13 ⁶ Department of Plant and Microbial Biology, University of California at Berkeley, Berkeley CA
14 USA

15 ⁷ Hollings Marine Lab, College of Charleston, Charleston SC, USA

16
17 †Present address: Department of Oceanography, University of Hawaii at Manoa, Honolulu HI

18
19 * Corresponding Authors. Contact: hawco@hawaii.edu, 1000 Pope Road, 808-956-2613;
20 msaito@whoi.edu, 266 Woods Hole Road MS#51, 508-289-2393.

21
22
23
24 Classification: Biological Sciences Ecology/Environmental Sciences/Evolution

25 Keywords: Cobalamin, iron, nutrient limitation, cyanobacteria, biogeochemical cycles

26
27
28 Short Title: *Prochlorococcus* minimum cobalt requirements

43
44
45
46
47
48
49
50
51
52
53
54
55
56
57
58
59
60
61
62
63
64
65
66
67
68
69
70
71
72
73

Abstract

Despite very low concentrations of cobalt in marine waters, cyanobacteria in the genus *Prochlorococcus* retain the genetic machinery for the synthesis and use of cobalt-bearing cofactors (cobalamins) in their genomes. We explored cobalt metabolism in a *Prochlorococcus* isolate from the Equatorial Pacific Ocean (strain MIT9215) through a series of growth experiments under iron and cobalt limiting conditions. Metal uptake rates, quantitative proteomic measurements of cobalamin-dependent enzymes, and theoretical calculations all indicate that *Prochlorococcus* MIT9215 can sustain growth with less than 50 cobalt atoms per cell, approximately 100-fold lower than minimum iron requirements for these cells (~5100 atoms per cell). Quantitative descriptions of *Prochlorococcus* cobalt limitation are used to interpret new observations of the cobalt distribution in the Equatorial Pacific Ocean, where surface concentrations are among the lowest measured globally but *Prochlorococcus* biomass is high. A low minimum cobalt quota ensures that other nutrients, notably iron, will be exhausted before cobalt can be fully depleted, helping to explain the persistence of cobalt-dependent metabolism in marine cyanobacteria.

74
75
76
77
78
79
80
81
82
83
84
85
86
87
88
89
90
91
92
93
94
95
96
97
98
99
100
101
102
103
104

Significance statement

Photosynthetic phytoplankton are the foundation of marine ecosystems. Their growth in the sunlit ocean depends on ample supply of over a dozen essential elements. Of these elemental nutrients, the metal cobalt is found at the lowest concentrations in seawater but it is unknown if cobalt scarcity impacts phytoplankton growth. We have measured minimum cobalt requirements of the photosynthetic bacterium *Prochlorococcus*, which flourishes in nutrient poor regions of the ocean where many other phytoplankton cannot survive. *Prochlorococcus* can grow with less than 50 cobalt atoms per cell, an extraordinarily small requirement that explains how this organism can persist in low-cobalt environments. These results enable predictions of how marine ecosystems respond to climate-driven changes in nutrient supply.

105

106 **Introduction**

107 Cobalt is the least abundant elemental nutrient in seawater, but this may not have always
108 been the case. In the modern ocean, cobalt scarcity develops from the oxidation of soluble Co^{2+}
109 to insoluble Co^{3+} by Mn-oxidizing bacteria, (1, 2) leaving behind a small pool of cobalt bound to
110 strong organic ligands. Mn- and Co-oxidizing reactions are inhibited at low O_2 , leading to the
111 buildup of cobalt observed in oxygen-depleted waters (3–6). Similar reasoning has suggested
112 that much higher cobalt inventories were found prior to the oxygenation of the oceans ~300
113 million years ago (7, 8). Greater access to cobalt in the ancient anoxic ocean may have
114 encouraged cobalt use in metalloenzymes, which evolved early in earth's history (9, 10).

115 Since the oxidation of the oceans, there has been evolutionary selection against cobalt use
116 over time, consistent with its decreasing availability (7, 11, 12). Eukaryotic genomes use cobalt
117 less frequently than those of bacteria and archaea and all eukaryotic organisms lack the ability
118 for the *de novo* synthesis of cobalamin (vitamin B_{12}) from cobalt ion (13–15). The adoption of
119 cobalamin-independent isoforms of methionine synthase, ribonucleotide reductase and other
120 enzymes has liberated land plants from cobalt dependence altogether (14, 16). Despite its
121 scarcity and the availability of substitutes, there are benefits to cobalt use, exemplified among
122 marine phytoplankton. For instance, 100-fold faster catalysis by cobalamin-dependent
123 methionine synthase, MetH, compared to cobalamin-independent methionine synthase, MetE,
124 allows for economization of nitrogen and other limiting resources (15, 17). Furthermore, Co^{2+}
125 ions can activate Zn-dependent metalloenzymes like carbonic anhydrase, improving growth
126 under Zn scarcity (18–20).

127 In the surface ocean, light inhibits bacterial Mn-oxidation (21), but cobalt uptake by
128 phytoplankton leads to the lowest concentrations at any depth, which can fall below 10^{-11} mol L^{-1}
129 (10 pM; (3, 6, 22)). There is growing evidence that the addition of cobalt or cobalamin to surface
130 waters can increase phytoplankton growth rates when added in conjunction with other nutrients
131 like iron and nitrogen (23–26). Yet, it is difficult to extrapolate these observations because the
132 cobalt requirements of some key phytoplankton taxa have not been quantified.

133 Emerging prior to the oxygenation of the oceans, marine cyanobacteria in the
134 *Prochlorococcus* and *Synechococcus* lineage differ from eukaryotic phytoplankton in that they
135 possess an absolute requirement for cobalt, independent of other nutrients like Zn (7, 18, 27, 28).

136 Despite their minimal genomes, which contain nearly half as many genes as other cyanobacterial
137 species (e.g. *Synechocystis*), all sequenced *Prochlorococcus* genomes have retained pathways for
138 the *de novo* biosynthesis of pseudocobalamin (psB₁₂), a structural analog of vitamin B₁₂ (29–31).
139 The dominant phytoplankton group in the subtropical and tropical oceans, *Prochlorococcus*
140 contributes a significant fraction of global primary production (32, 33), but the amount of cobalt
141 needed to support this productivity is unknown. Here, we show that *Prochlorococcus* cells can
142 grow with a very small number of cobalt atoms, enabling this organism to thrive in cobalt poor
143 environments like the Equatorial Pacific Ocean without replacing cobalt-dependent metabolism.

144

145 **Results and Discussion**

146 ***Low cobalt and iron requirements of Prochlorococcus MIT9215***

147 To quantify cellular cobalt requirements, we conducted growth experiments in
148 chemically defined media with axenic cultures of *Prochlorococcus* strain MIT9215, a member of
149 the abundant high-light II clade that was originally isolated from the Equatorial Pacific Ocean
150 (34). While scarce iron in this region limits the growth of *Prochlorococcus* and other
151 phytoplankton (35, 36), the tropical Pacific Ocean also hosts low cobalt concentrations (< 10 pM
152 (3, 23, 37)).

153 The influence of nutrient limitation on fitness is a function of two distinct traits: 1) the
154 ability of a cell to acquire nutrients from seawater and 2) the ability to apply acquired nutrients
155 toward the biosynthesis of compounds needed for growth and cell division (38). In our
156 experiments, division rates of *Prochlorococcus* MIT9215 decreased when inorganic cobalt
157 concentrations (Co', see methods) fell below 3 pM and no growth was observed at a Co'
158 concentration below 0.1 pM (Fig. 1A). However, thresholds of Co' in these experiments were
159 highly sensitive to the concentrations of Zn and Mn present in the growth medium, due to
160 competitive inhibition at the uptake site and are difficult to relate to typical oceanic
161 concentrations directly (39). Regardless, we observed a robust relationship between intracellular
162 cobalt contents (the cobalt quota, Q_{Co}) and cell growth rate (μ , Figs. 1B, S1). Growth of
163 *Prochlorococcus* MIT9215 was well described by the Droop Equation:

$$164 \quad \mu = \mu_{max} \left(1 - \frac{q_{min}}{Q_{Co}} \right) \quad (1)$$

165 which derives an absolute minimum quota, q_{min} , as growth rate (μ) approaches 0 (38). Least-
166 squares fitting of q_{min} yielded extraordinarily low values: 14.8 ± 1.3 atoms per cell ($R^2 = 0.96$;

167 equivalent to a cellular concentration of 220 nM). Implicit in this model is the expectation that
168 increasing growth rates must be fueled by higher cobalt quotas, which is supported by our
169 observations (Fig. 1B). From Eq. 1, a growth-limited range ($\mu < 95\% \mu_{max}$, Table S1) can be
170 identified when the cellular cobalt quota is approximately 300 atoms per cell or less, equal to a
171 Co:Carbon ratio of $1.2 \pm 0.1 \times 10^{-7}$ (atom:atom). This value is similar to the Co:C ratio of a
172 coastal *Synechococcus* under cobalt limitation (0.8×10^{-7} (18)), but an order of magnitude lower
173 than the composite Co:C of eukaryotic phytoplankton (1.5×10^{-6} (40)), which is biochemically
174 distinct from the cyanobacterial requirement and reflects variable substitution with Zn (18).

175 Cellular cobalt demands were compared to those of iron, the nutrient that limits
176 *Prochlorococcus* growth in the Equatorial Pacific Ocean (36). Growth limitation occurred when
177 inorganic iron concentrations (Fe^{2+}) fell below 30 pM (Fig. 1A), similar to dissolved iron
178 concentrations in the Equatorial Pacific (41). To avoid iron limitation, *Prochlorococcus*
179 MIT9215 required upwards of $31,000 \pm 3400$ Fe atoms per cell ($\mu < 95\% \mu_{max}$, $R^2 = 0.96$, Table
180 S1) and estimated Fe:C ratios of iron limited cells ($1.6 \pm 0.2 \times 10^{-5}$) were similar to Fe:C ratios of
181 bulk particulate digestions from the Equatorial Pacific, the closest approximation of
182 *Prochlorococcus* metal quotas *in situ* (42). Iron requirements in *Prochlorococcus* MIT9215 were
183 much lower than those reported for *Prochlorococcus* strain MED4 ($Fe:C > 4.1 \times 10^{-5}$), which
184 was isolated from the iron-rich Mediterranean Sea (43, 44), suggesting evolutionary pressure
185 within this group to adapt to iron-poor regions of the oceans. The low Fe quotas of
186 *Prochlorococcus* MIT9215 are still 100-fold larger than minimum cobalt requirements measured
187 here (Fig. 1B, Table S1).

188

189 ***Cobalt use efficiency in Prochlorococcus***

190 Raven (1988) originally defined a ‘metal use efficiency’ by scaling *in vitro* enzyme rates
191 with protein:metal stoichiometries to derive maximum rates of biomass production per atom of
192 catalytic metal (45, 46). For example, given light-saturated rates of O_2 evolution at photosystem
193 II and a stoichiometry of 20 iron atoms per photosynthetic unit (Table S3), a photoautotrophic
194 cell could be expected to grow at a rate of 1 mol C per second, per mol Fe (45). At this iron use
195 efficiency, a cell the size of *Prochlorococcus* growing at a rate 0.4 per day would need ~8200
196 iron atoms per cell, similar to measured iron quotas at this growth rate (5100 ± 1100 atoms per

197 cell, Table S2). This is consistent with photosynthetic and respiratory enzymes being the
198 dominant use for acquired iron in *Prochlorococcus*.

199 We sought to extend this metal use efficiency framework to cobalt. All sequenced
200 *Prochlorococcus* genomes encode two cobalamin-dependent enzymes: 1) the ribonucleotide
201 triphosphate reductase NrdJ, which generates deoxyribonucleotide bases (dNTPs) for DNA
202 replication from ribonucleotide precursors, and 2) the methionine synthase MetH, which
203 methylates homocysteine to generate the amino acid methionine, needed for protein synthesis
204 (30, 47). Unlike plants and many eukaryotic phytoplankton (15), *Prochlorococcus* lack
205 cobalamin-independent versions of ribonucleotide reductase and methionine synthase, indicating
206 that there is no substitute for cobalt requirements associated with NrdJ and MetH. Other
207 characterized cobalamin or Co^{2+} dependent enzymes, such as methylmalonyl CoA mutase and
208 nitrile hydratase, are not present in the genome of *Prochlorococcus* MIT9215 or other sequenced
209 *Prochlorococcus* strains.

210 Prior to dividing, *Prochlorococcus* MIT9215 must replicate its genome of 1.7 million
211 base pairs, requiring dNTP synthesis via NrdJ. To grow at a rate of 0.6 per day, the maximum
212 observed in our experiments and similar to *in situ* growth rates in the Equatorial Pacific (36), at
213 least 2.04 million dNTP bases per cell must be synthesized daily. *In vitro* characterizations of
214 NrdJ show a maximum turnover time of 2 cycles per second: unimpeded, a single enzyme can
215 produce 170,000 dNTP bases per day (48, 49). Assuming that the *Prochlorococcus* NrdJ can
216 achieve similar rates *in vivo*, cellular demand for dNTPs would require at least 12 functioning
217 copies of this enzyme to support maximum growth rates (Table S4).

218 A much faster enzyme, MetH can operate at over 18 cycles per second (17, 50). A single
219 MetH enzyme can produce over 1.5 million methionine molecules per day. While a complex
220 methionine cycle makes it challenging to predict cellular MetH demands (51), the cellular sulfur
221 quota of roughly 12 million atoms (composed of methionine, cysteine and homocysteine thiols,
222 sulfates, and sulfones, etc.) can serve as an upper bound (Table S4). By this calculation, 5 copies
223 of MetH would fulfill even this overestimated demand.

224 Given a 1:1 protein:cobalt stoichiometry evident from crystal structures of NrdJ and
225 MetH, this analysis can account for 17 Co atoms in cobalamin dependent enzymes for
226 *Prochlorococcus* growing maximally, equivalent to a metal use efficiency of 6.6×10^7 mol C per
227 day per mol Co. This estimate is 4-fold higher than empirical Co use efficiencies of 1.6×10^7

228 calculated from growth experiments (Table S1, S4), which may indicate the presence of
229 additional Co associated with unknown enzymes, chaperones and other transient reservoirs
230 within the cell. To a first order, however, these calculations suggest that the quotas measured in
231 *Prochlorococcus* cells are biochemically reasonable.

232

233 ***Mass balance of cobalt metabolism***

234 To validate the above calculations, we constructed ¹⁵N-labeled peptide standards to
235 quantify intracellular NrdJ and MetH levels by selected reaction monitoring mass spectrometry.
236 From large volume cultures of cobalt-limited *Prochlorococcus* MIT9215 ($\mu = 0.2 \text{ day}^{-1}$),
237 measurements of 4 tryptic peptides indicated that there were 15 ± 2 copies of NrdJ per cell (Fig.
238 1C, Tables S5-S7). In the same sample, MetH was measured to an abundance of 7 ± 2 copies per
239 cell. These measurements are remarkably consistent with predictions of 5 MetH and 12 NrdJ
240 copies per cell based on the above use efficiency calculations at peak growth rates.

241 Still, the maximum amount of cobalt that can be attributed to use in NrdJ and MetH
242 enzymes (22 ± 3 atoms per cell, assuming a 1:1 stoichiometry between Co and enzyme) is
243 significantly less than the total cobalt quota in these cells, as measured by ICP-MS (62 ± 7 atoms
244 per cell; Fig. 1C). Other reservoirs may account for more cobalt than NrdJ and MetH, even at
245 these low intracellular concentrations. Before being used in NrdJ and MetH, acquired Co^{2+} ions
246 must be transformed into pseudocobalamin (psB₁₂) cofactors, whose biosynthesis requires over a
247 dozen enzymatic steps, beginning with the insertion of Co^{2+} into the corrinoid ring by the
248 cobaltochelatase CbiK (14). Given that many of psB₁₂ biosynthetic intermediates would be
249 present at a steady-state concentration of a few copies per cell or less, the random walks of single
250 molecules from the active site of one enzyme in the biosynthetic sequence to the next may be the
251 rate limiting step to *Prochlorococcus* growth under cobalt limitation. The sheer number of
252 enzymatic alterations required to produce pseudocobalamin (>15 cobalt-bearing intermediates
253 (12, 45)) probably acts as a limit to growth efficiency at low cobalt.

254 Perhaps related to these physical limits, there appears to be a lack of regulatory control on
255 *Prochlorococcus* MIT9215 cobalt metabolism, at least by inorganic Co species. The abundance
256 of NrdJ and MetH did not increase significantly at higher Co' abundance, despite a 14-fold
257 increase in cellular Co ($54\text{--}780 \text{ atoms cell}^{-1}$; Fig. S2A). Cobalt use efficiency calculations imply
258 that the measured cellular inventory of NrdJ and MetH in cobalt-limited cells is sufficient to

259 sustain the flux of dNTP and methionine needed to support maximum growth rates. When
260 cellular cobalt quotas are growth-limiting, it is likely that these enzymes are unsaturated with
261 respect to their pseudocobalamin cofactors, decreasing their metabolic production and delaying
262 cell division.

263 Furthermore, comparisons between the cellular proteomes of replete and cobalt-limited
264 *Prochlorococcus* MIT9215 did not show large differences in protein abundance, with only 12%
265 of detected proteins significantly different (Fig. S2B). Stress-related proteins – the
266 photosynthetic proteins PsaD, PsbO, and some ribosomal proteins – were somewhat higher in
267 cobalt-limited cells while ATP synthase and sugar metabolism genes were less abundant (Table
268 S8). As these proteins are associated with basic metabolic functions, it is likely that changes in
269 the cell division rate, not cobalt itself, drive differences in the proteome under cobalt-limiting
270 conditions. This is consistent with the absence of many cyanobacterial metal sensing and
271 regulatory genes in *Prochlorococcus* genomes (39, 53).

272

273 ***Prochlorococcus* Co nutrition in the Equatorial Pacific Ocean**

274 All sequenced *Prochlorococcus* isolates harbor genes for psB₁₂ synthesis, as well as *nrdJ*
275 and *metH*. It is expected that the cobalt requirements defined for the MIT9215 strain are broadly
276 representative of all *Prochlorococcus* cells – at least as a lower limit – and can be used to
277 investigate whether wild *Prochlorococcus* populations can meet their nutritional cobalt
278 requirements.

279 To this end, we mapped the distribution of cobalt in the Equatorial Pacific Ocean – the
280 region where *Prochlorococcus* MIT9215 was originally isolated – from samples collected on the
281 Metzyme expedition in October 2011 (Fig. 2A). Dissolved cobalt was depleted in the surface
282 ocean and accumulated in mesopelagic waters, consistent with the distribution of other
283 phytoplankton nutrients like phosphate (Fig. 2B-D). In the subsurface, cobalt concentrations
284 greater than 100 pmol L⁻¹ were associated with very low oxygen waters (<50 μM; Fig. 2E, S3A)
285 that extend all the way to the eastern margin (3). Sustained anoxia along the continental shelves
286 of Peru and Mexico promotes the dissolution of cobalt bound in sedimentary Mn-oxides (54, 55),
287 and, at the basin scale, cobalt input from these reducing sediments is balanced by its removal
288 onto Mn-oxides formed in oxic waters (56). Inhibition of Mn and Co oxidation at low O₂,

289 combined with significant regeneration of phytoplankton-derived cobalt, leads to plumes of high
290 cobalt within low oxygen waters in both the North and South Pacific (Fig. 2C).

291 At the equator, upwelling of subsurface waters from the Equatorial Undercurrent (EUC)
292 leads to high nutrient concentrations and productivity. Originating in the oxygenated waters of
293 the western Pacific, the EUC transports a large iron source from Papua New Guinea into the
294 equatorial upwelling region (41, 57). As it travels eastward, the EUC splits low oxygen water
295 masses, leading to a downward deflection of O₂ contours between 2°N and 2°S (Fig. 2B) (58).
296 Despite its importance as an iron source, cobalt concentrations within the EUC were not elevated
297 (30 ± 2 pM between 100–250 m), especially compared to the surrounding low oxygen waters
298 (Fig. 2C). Low cobalt in the EUC probably reflects the high O₂ concentrations near Papua New
299 Guinea and the predominance of oxic (rather than reducing) sedimentary sources (57, 59).
300 Instead, entrainment of low oxygen, high cobalt waters into the EUC leads to elevated cobalt
301 concentrations in the euphotic zone at the equator (23 ± 6 pM over 0–100 m; Fig. 2C).

302 As upwelled equatorial waters are advected poleward, nutrient concentrations throughout
303 the euphotic zone decrease due to uptake by phytoplankton. Interestingly, cobalt is more strongly
304 depleted in the South Pacific Gyre than in the North Pacific, opposite to the trend in phosphate
305 (compare, for instance, the 5 pM contour for cobalt in Fig. 2B and the 0.25 μM contour for PO₄
306 in Fig. 2C). Greater contact with coastal sources from East Asia, a larger oxygen minimum zone,
307 as well as orders of magnitude greater deposition of desert dust in the northern hemisphere
308 probably contribute to higher cobalt inventories in the North Pacific Subtropical Gyre (60–62).
309 These sources are weaker in the South Pacific, allowing surface concentrations to fall below the
310 2 pM detection limit of our electrochemical method at both 9.2°S and 12°S (Fig. 3A). These
311 stations also contained the largest populations of *Prochlorococcus* observed on the transect,
312 evident in divinyl chlorophyll *a* concentrations (which are specific to *Prochlorococcus* (63)) that
313 exceeded chlorophyll *a* produced by other phytoplankton (Fig. S4). At a threshold growth rate of
314 95% μ_{max}, cobalt requirements of *Prochlorococcus* MIT9215 are estimated to be 300 atoms cell⁻¹,
315 equivalent to a biomass Co:P ratio of 26×10^{-6} (Table S1). Thus, in order to take up the 300
316 nM of surface PO₄ found at 9.2°S and 12°S, *Prochlorococcus* must also acquire at least 7.8 pM
317 Co in order to avoid cobalt-limited growth rates: more than triple the dCo concentration found at
318 these stations. Indeed, dissolved Co:PO₄ ratios in the euphotic zone (0–100 m) fall below this

319 threshold for all stations south of the Equator (Fig. 3E), suggesting that the PO₄ reservoir here
320 cannot be depleted without forcing cobalt-limited growth rates.

321 However, elemental standing stocks do not always reflect their availability to organisms,
322 many of which are adept at recycling trace nutrients. In the South Pacific, depletion of cobalt
323 from the dissolved phase of seawater observed on the Metzyme expedition is mirrored by a
324 significant accumulation of cobalt in particulate matter, often exceeding 1 pM (Fig. 3C).
325 Correlation between pCo and particulate phosphate (pP) indicates that pCo is primarily
326 associated with biomass (Fig. 3D, S3B). In both the North and South Pacific, the Co:P
327 composition of particulate matter ($110 \pm 30 \times 10^{-6}$) exceeds both dissolved Co:PO₄ ratios and
328 cobalt limitation thresholds of *Prochlorococcus* MIT9215 identified in culture (26×10^{-6} ; Fig.
329 3E). To the extent that the Co:P composition of the total particulate pool reflects the composition
330 of *Prochlorococcus* cells, it would appear that wild *Prochlorococcus* populations in the South
331 Pacific have accumulated enough cobalt to satisfy their cobalamin metabolism and avoid cobalt
332 limitation.

333 To understand how phytoplankton are able to accumulate Co in this region, we analyzed
334 a global model of the marine cobalt cycle (37), which reproduces the very low dissolved cobalt
335 concentrations observed in the South Pacific but does not contain explicit parameterizations for
336 Co limitation of phytoplankton growth. In the model, the South Pacific Gyre is the only region
337 where dissolved Co:PO₄ ratios fall below the 95% μ_{\max} threshold for *Prochlorococcus* MIT9215
338 (excluding the Southern Ocean where waters are too cold to support *Prochlorococcus* growth
339 (64)). Similar to our observations, the model also simulates elevated phytoplankton Co:P ratios
340 in the South Pacific Gyre ($>100 \times 10^{-6}$), along with low dissolved Fe concentrations and Fe
341 limitation of phytoplankton growth (Fig. S5, S6). Conceptually, iron-limited growth would allow
342 the same number of cobalt transporters to complete more transport cycles prior to cell division,
343 leading to a build-up of cellular Co. This effect is responsible for elevated phytoplankton Co:P
344 ratios in the model, and was also observed during our iron limitation experiments with
345 *Prochlorococcus* MIT9215 in culture (Fig. S1, Table S2). High levels of iron transporters and
346 other protein biomarkers observed during the Metzyme expedition support model-based
347 conclusions that iron limits *Prochlorococcus* growth in the South Pacific Gyre (Fig. S7; (35)).
348 Thus, cobalt accumulation afforded by iron-limited growth may be responsible for the high
349 particulate Co:P ratios also observed on this transect.

350 Analysis of the measurements within the GEOTRACES intermediate data product (65)
351 yields a similar conclusion: all waters with low Co:PO₄ ratios also contain comparably lower
352 Fe:PO₄ ratios (with respect to q_{min} values of Fe and Co determined from culture experiments, Fig.
353 4). If *Prochlorococcus* growth thresholds for cobalt and iron are assumed to be independent of
354 one another (as in Liebig's law of the minimum), then cobalt limitation will be blocked by iron
355 limitation (Fig. 4). Still, this scenario suggests that iron addition on short timescales (e.g. dust
356 deposition) may drive *Prochlorococcus* and other phytoplankton toward cobalt limitation,
357 consistent with observations of iron and cobalt co-limitation in bottle incubations (23, 25).

358 There are two factors that complicate this interpretation. First, some *Prochlorococcus*
359 lineages may retain a higher Co requirement than *Prochlorococcus* MIT9215, due to a reliance
360 on other putative Co-dependent metalloenzymes, such as the PhoA alkaline phosphatase (30,
361 66). Second, in addition to *Prochlorococcus*, the pool of particulate matter in the surface ocean is
362 also composed of small eukaryotic phytoplankton, mixotrophs, and grazers, as well as
363 heterotrophic bacteria and detritus. Differences in cobalt (or P) accumulation between these
364 reservoirs will distort comparisons with axenic *Prochlorococcus* cultures. Indeed, the cobalt
365 requirements of eukaryotic phytoplankton like the diatom *Thalassiosira oceanica* and the
366 haptophyte *Emiliana huxleyi* can be much greater than *Prochlorococcus* MIT9215 (Co:C >10⁻⁶
367 for both species) because these organisms substitute cobalt into their Zn-dependent enzymes
368 (cambialism) when grown under low zinc concentrations found in open ocean environments (18,
369 19). Under conditions of Zn scarcity, the Co requirements of *E. huxleyi* can be more than 10-fold
370 higher than *Prochlorococcus* MIT9215: equivalent to a biomass Co:P ratio greater than 300 x 10⁻⁶
371 (67). While the degree of Co-Zn inter-replacement in the open ocean is currently unknown,
372 dissolved Zn in the South Pacific Gyre can fall below 0.1 nM (65), and free Zn' concentrations
373 are likely orders of magnitude lower due to complexation by organic ligands (69). When
374 analyzing the Co:P ratio of a mixed assemblage, the potentially high Co:P ratios associated with
375 cambialistic requirements may mask lower *Prochlorococcus* Co:P. Such high Co requirements
376 must also make eukaryotic phytoplankton more susceptible to Co-Zn limitation. At the Co:P
377 stoichiometry observed in *E. huxleyi*, the severity of Co depletion would exceed Fe throughout
378 large areas of the North and South Pacific Oceans (Fig. 4, S8), possibly leading to Co-Zn
379 limitation of growth. The simultaneous depletion of iron, nitrogen, cobalt, zinc, and other

380 nutrients in the South Pacific and other subtropical gyres may prevent large scale increases in
381 ecosystem biomass, even if sources of the ‘limiting’ nutrient are increased.

382

383 ***Evolutionary drivers of minimized cobalt metabolism***

384 High cobalt concentrations in the Equatorial Pacific are associated with oxygen-poor
385 water masses, matching observations elsewhere in the Pacific and Atlantic (3, 6, 70). The
386 worldwide association between Co and O₂ supports thermodynamic predictions that the anoxic
387 ocean found during the Proterozoic and Archaean also contained much higher cobalt (7). As
388 cyanobacteria evolved during this time, high cobalt availability probably facilitated the
389 incorporation of (pseudo)cobalamin-dependent enzymes like NrdJ and MetH instead of other,
390 cobalamin-independent versions of these proteins. However, genome-based timelines suggest
391 that the *Prochlorococcus* lineage did not emerge until the late Paleoproterozoic or early
392 Phanerozoic (28, 71). Although marine oxygen concentrations during this period are uncertain,
393 the subsequent diversification of *Prochlorococcus* ecotypes throughout the Phanerozoic probably
394 occurred in an oxygenated ocean (28, 72), with cobalt concentrations that were probably lower
395 than when the cyanobacteria first evolved. As the evolution of *Prochlorococcus* ecotypes is
396 characterized by metabolic streamlining and genome minimization (73, 74), it is interesting to
397 note that, because all DNA bases in *Prochlorococcus* are synthesized by the NrdJ enzyme,
398 decreasing genome size also helps to decrease cobalt requirements.

399 Our analysis suggests that *Prochlorococcus* cells can continue to function with a very
400 small number of cobalt atoms, as low as 17 atoms per cell. While some lineages of
401 *Prochlorococcus* may maintain a broader suite of cobalt-dependent or cambialistic enzymes (and
402 therefore a higher cobalt requirement), the very low cobalt requirement of *Prochlorococcus*
403 MIT9215 minimizes its exposure to cobalt-limiting conditions (Fig. 4), likely explaining the
404 retention of psB₁₂ biosynthesis in *Prochlorococcus* genomes. Similarity in proteomes between
405 cobalt-replete and cobalt-limited growth suggests that *Prochlorococcus* MIT9215 does not
406 actively monitor its cobalt inventory (Fig. S2), nor does it make significant efforts to increase Co
407 uptake by upregulating Co’ transport systems. Indeed, Co’ uptake into *Prochlorococcus*
408 MIT9215 cells appears to be relegated to the periplasmic Mn transport system MntABC, rather
409 than a transporter specific to cobalt (39). These adaptations may reflect efforts to decrease the
410 number of transporters and regulatory systems needed within the cell, a resource and energy

411 savings that may offset the resource/energy expenditure associated with the production of psB₁₂
412 biosynthetic enzymes.

413 While all sequenced *Prochlorococcus* genomes have retained the genes for psB₁₂
414 biosynthesis, there are other cyanobacteria that have lost this functionality. For example, the
415 benthic cyanobacterium *Synechococcus* PCC7002 has lost its cobalamin biosynthetic pathway
416 and replaced its ancestral *nrdJ* with horizontally-acquired *nrdAB* genes, which encode a B₁₂-
417 independent ribonucleotide reductase (75, 76). As a result, *Synechococcus* PCC7002 depends on
418 exogenous B₁₂ to power the MetH methionine synthase. Genetic replacement of the *metH* gene
419 with B₁₂-independent methionine synthase, *metE*, is sufficient to relieve *Synechococcus*
420 PCC7002 of its B₁₂ dependence (75). Several other cyanobacteria (e.g. *Synechococcus*
421 PCC73109, *Crocospaera watsonii*) have also acquired B₁₂-independent versions of both
422 methionine synthase and ribonucleotide reductase. Given pervasive signals of horizontal gene
423 acquisition in *Prochlorococcus* genomes (74), it is surprising that *metE* and *nrdAB* genes are
424 absent from sequenced *Prochlorococcus* isolates.

425 *Prochlorococcus* appears to retain its psB₁₂-dependent enzymes out of physiological
426 benefit rather than an insufficient access to B₁₂-independent alternatives. The cobalamin-
427 independent ribonucleotide reductase NrdAB is an iron-dependent enzyme (77), whose
428 incorporation would require an increase in *Prochlorococcus*'s iron requirement, making it less
429 competitive in iron-limited waters. Similarly, B₁₂-independent MetE can only operate at ~1% the
430 rate of MetH, and would therefore be needed at much higher quantity (15, 17), increasing
431 demand for photosynthate (and therefore for Fe). Eukaryotic phytoplankton with both *metE* and
432 *metH* genes clearly prefer to use MetH when B₁₂ is present (15). The sheer abundance of
433 *Prochlorococcus* throughout the subtropics and tropics implies that it is the major synthesizer of
434 cobalamins throughout the sunlit ocean (29, 78, 79), and therefore supports the B₁₂ dependencies
435 of other phytoplankton (the pseudocobalamin produced by *Prochlorococcus* being convertible to
436 conventional B₁₂ by many species (29, 80)). The persistence of psB₁₂ biosynthesis in
437 *Prochlorococcus* not only makes its own metabolism more efficient, but potentially the entire
438 marine ecosystem.

439 Partially degraded B₁₂ and psB₁₂ molecules are inferred to be the major source of
440 dissolved cobalt ligands found in seawater, whose stability over hundreds of years protects cobalt
441 in the ocean interior from scavenging by Mn-oxidizing bacteria and burial in marine sediments

442 (23, 37, 56). Therefore, minimization – rather than replacement – of *Prochlorococcus*
443 cobalamin-dependent metabolism may have a global effect on the marine cobalt cycle.

444

445 **Methods**

446 Axenic cultures of *Prochlorococcus* MIT9215 were grown, harvested and analyzed as
447 described previously (39). Growth rates were determined in multiple 30 mL polycarbonate tubes
448 and pooled to measure cellular metal quotas and protein content. Large (8L) non-axenic cultures
449 were used to grow biomass for quantitative protein measurements.

450 Global and targeted protein measurements were measured following previously described
451 protocols (35, 81). Significantly different protein abundance was determined by the Fisher exact
452 test using a cut-off of $p < 0.01$. Concentrations of *Prochlorococcus* MIT9215 ribonucleotide
453 reductase (NrdJ) and methionine synthase (MetH) were measured in soluble protein extracts
454 using ^{15}N labeled peptide standards generated from *Prochlorococcus* NrdJ and MetH peptides in
455 an *E. coli* overexpression system. Labeled peptides were co-expressed with a peptide sequences
456 for horse myoglobin which were calibrated relative to a commercially available horse myoglobin
457 protein (Fisher). Presence/absence of *nrdA*, *nrdJ*, *metE*, and *metH*, was determined by BLASTp
458 searches with E-value cutoffs of 10^{-20} .

459 Dissolved cobalt concentrations (operationally defined as passing through a $0.2\ \mu\text{m}$ filter)
460 from the Metzyme expedition (KM1128) were measured by cathodic stripping voltammetry (3,
461 35) and available at the Biological and Chemical Oceanography Data Management Office
462 repository (BCO-DMO, Dataset #647250). Sampling procedures and analysis of particulate
463 metals is described by Saito et al. 2014 (35). Equations governing the Co biogeochemical model
464 can be found elsewhere (37). Expanded methodological details can be found in the
465 supplementary information.

466

467 **Acknowledgements**

468 We are grateful for the Captain and Crew of the R/V Kilo Moana for their assistance on the
469 KM1128 expedition, co-chief scientist Carl Lamborg. We thank John Waterbury for allowing us
470 access to incubators, as well as Alison Coe and the Chisholm lab at MIT for providing
471 *Prochlorococcus* cultures. We also thank Elizabeth Kujawinski, Mick Follows, Phoebe Lam and
472 three anonymous reviewers for constructive feedback on this work. This work was supported by

473 the Gordon and Betty Moore Foundation grants 3782 and 3934 to MAS, and National Science
474 Foundation awards OCE-1031271, OCE-1220484, OCE-1337780 to MAS. The writing of the
475 manuscript was supported by a Simons Foundation Life Sciences Postdoctoral Fellowship to
476 NJH (602538).

477

478 **Author Contribution Statement**

479 NJH MRM, RMB and MAS designed laboratory experiments, which were performed by NJH,
480 MRM, RMB, and LVA. NJH, MRM, GRD, DMM, MAS and TJG collected samples and
481 measured parameters from the KM1128 cruise. AT, NJH, RMB, and MAS analyzed model
482 results. This manuscript was written by NJH and MAS with contributions from all authors.

483

484 **References**

485

- 486 1. Moffett JW, Ho J (1996) Oxidation of cobalt and manganese in seawater via a common
487 microbially catalyzed pathway. *Geochim Cosmochim Acta* 60(18):3415–3424.
- 488 2. Lee B, Fisher NS (1993) Microbially mediated cobalt oxidation in seawater revealed by
489 radiotracer experiments. *Limnol Oceanogr* 38(8):1593–1602.
- 490 3. Hawco NJ, Ohnemus DC, Resing JA, Twining BS, Saito MA (2016) A cobalt plume in
491 the oxygen minimum zone of the Eastern Tropical South Pacific. *Biogeosciences*
492 13:5697–5717.
- 493 4. Ohnemus DC, et al. (2017) Elevated trace metal content of prokaryotic plankton
494 communities associated with marine oxygen deficient zones. *Limnol Oceanogr* 62(1):3–
495 25.
- 496 5. Johnson KS, Coale KH, Berelson WM, Michael Gordon R (1996) On the formation of the
497 manganese maximum in the oxygen minimum. *Geochim Cosmochim Acta* 60(8):1291–
498 1299.
- 499 6. Noble AE, et al. (2012) Basin-scale inputs of cobalt, iron, and manganese from the
500 Benguela-Angola front to the South Atlantic Ocean. *Limnol Oceanogr* 57(4):989–1010.
- 501 7. Saito MA, Sigman DM, Morel FM. (2003) The bioinorganic chemistry of the ancient
502 ocean: the co-evolution of cyanobacterial metal requirements and biogeochemical cycles
503 at the Archean–Proterozoic boundary? *Inorganica Chim Acta* 356:308–318.
- 504 8. Swanner ED, et al. (2014) Cobalt and marine redox evolution. *Earth Planet Sci Lett*
505 390:253–263.
- 506 9. Weiss MC, et al. (2016) The physiology and habitat of the last universal common
507 ancestor. *Nat Microbiol* 1(9):1–8.
- 508 10. Lundin D, Berggren G, Logan DT, Sjöberg B (2015) The Origin and Evolution of
509 Ribonucleotide Reduction. *Life* 5(1):604–636.
- 510 11. Dupont CL, Butcher A, Valas RE, Bourne PE, Caetano-Anollés G (2010) History of
511 biological metal utilization inferred through phylogenomic analysis of protein structures.
512 *Proc Natl Acad Sci* 107(23):10567–10572.
- 513 12. da Silva JJRF, Williams RJP (1991) *The Biological Chemistry of the Elements: The*

- 514 *Inorganic Chemistry of Life* (Oxford University Press, Oxford, 1991).
- 515 13. Dupont CL, Yang S, Palenik B, Bourne PE (2006) Modern proteomes contain putative
516 imprints of ancient shifts in trace metal geochemistry. *Proc Natl Acad Sci U S A*
517 103(47):17822–17827.
- 518 14. Rodionov D a, Vitreschak AG, Mironov A a, Gelfand MS (2003) Comparative genomics
519 of the vitamin B12 metabolism and regulation in prokaryotes. *J Biol Chem*
520 278(42):41148–59.
- 521 15. Bertrand EM, et al. (2013) Methionine synthase interreplacement in diatom cultures and
522 communities : Implications for the persistence of B 12 use by eukaryotic phytoplankton.
523 *Limnol Oceanogr* 58(4):1431–1450.
- 524 16. Zhang Y, Rodionov DA, Gelfand MS, Gladyshev VN (2009) Comparative genomic
525 analyses of nickel, cobalt and vitamin B12 utilization. *BMC Genomics* 10:78.
- 526 17. Banerjee R V, Frasca V, Ballou DP, Matthews RG (1990) Participation of cob(I) alamin
527 in the reaction catalyzed by methionine synthase from *Escherichia coli*: a steady-state and
528 rapid reaction kinetic analysis. *Biochemistry* 29(50):11101–9.
- 529 18. Sunda WG, Huntsman SA (1995) Cobalt and zinc interreplacement in marine
530 phytoplankton: Biological and geochemical implications. *Limnol Oceanogr* 40(8):1404–
531 1417.
- 532 19. Yee D, Morel FMM (1996) In vivo substitution of zinc by cobalt in carbonic anhydrase of
533 a marine diatom. *Limnol Oceanogr* 41(3):573–577.
- 534 20. Price NM, Morel FMM (1990) Cadmium and cobalt substitution for zinc in a marine
535 diatom. *Nature* 344(6267):658–660.
- 536 21. Sunda WG, Huntsman S A. (1988) Effect of sunlight on redox cycles of manganese in the
537 southwestern Sargasso Sea. *Deep Sea Res Part A Oceanogr Res Pap* 35(8):1297–1317.
- 538 22. Noble AE, Saito MA, Maiti K, Benitez-Nelson CR (2008) Cobalt, manganese, and iron
539 near the Hawaiian Islands: A potential concentrating mechanism for cobalt within a
540 cyclonic eddy and implications for the hybrid-type trace metals. *Deep Sea Res Part II Top*
541 *Stud Oceanogr* 55(10–13):1473–1490.
- 542 23. Saito MA, Rocap G, Moffett JW (2005) Production of cobalt binding ligands in a
543 *Synechococcus* feature at the Costa Rica upwelling dome. *Limnol Oceanogr* 50(1):279–
544 290.
- 545 24. Bertrand EM, et al. (2007) Vitamin B 12 and iron colimitation of phytoplankton growth in
546 the Ross Sea. *Limnol Oceanogr* 52(3):1079–1093.
- 547 25. Browning TJ, et al. (2017) Nutrient co-limitation at the boundary of an oceanic gyre.
548 *Nature* 551:242.
- 549 26. Martin JH, Gordon RM, Fitzwater S, Broenkow WW (1989) Vertex: phytoplankton/iron
550 studies in the Gulf of Alaska. *Deep Sea Res Part A Oceanogr Res Pap* 36(5):649–680.
- 551 27. Saito MA, Moffett JW, Chisholm SW, Waterbury JB (2002) Cobalt limitation and uptake
552 in *Prochlorococcus*. *Limnol Oceanogr* 47(6):1629–1636.
- 553 28. Sánchez-Baracaldo P (2015) Origin of marine planktonic cyanobacteria. *Sci Rep* 5:17418.
- 554 29. Heal KR, et al. (2016) Two distinct pools of B₁₂ analogs reveal community
555 interdependencies in the ocean. *Proc Natl Acad Sci* 114(2):201608462.
- 556 30. Biller SJ, et al. (2014) Genomes of diverse isolates of the marine cyanobacterium
557 *Prochlorococcus*. *Sci Data* 1:1–11.
- 558 31. Rocap G, et al. (2003) Genome divergence in two *Prochlorococcus* ecotypes reflects
559 oceanic niche differentiation. *Nature* 424(6952):1042–7.

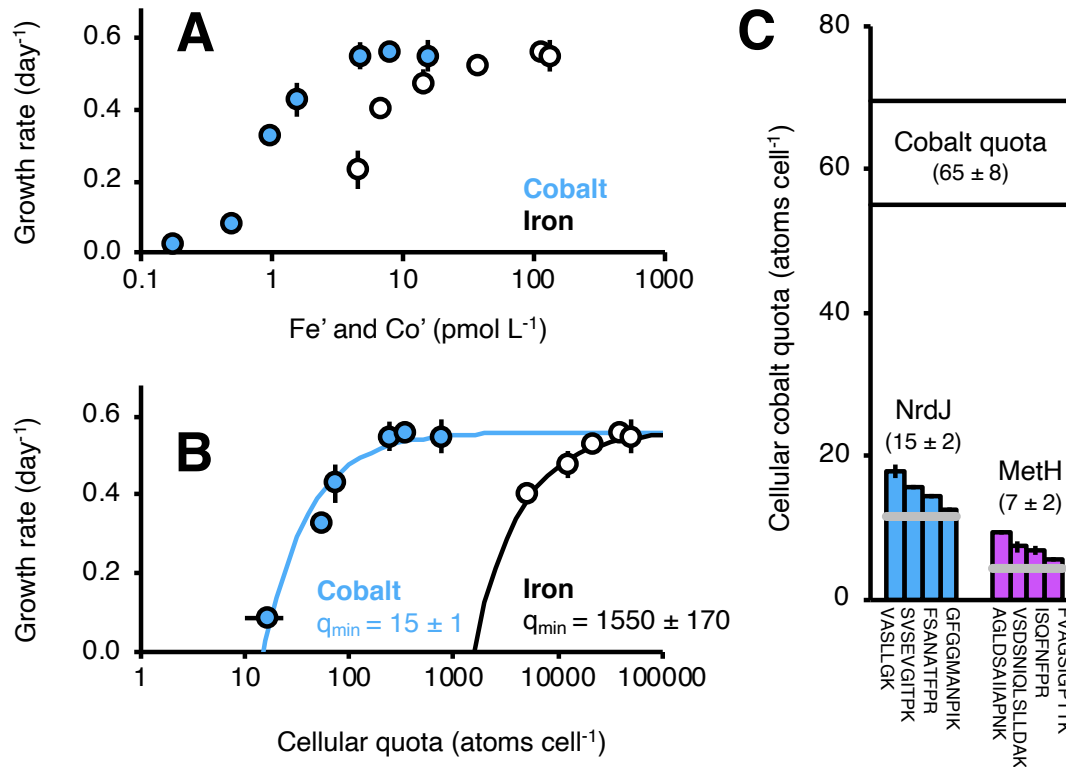
- 560 32. Rii YM, Karl DM, Church MJ (2016) Temporal and vertical variability in
561 picophytoplankton primary productivity in the North Pacific Subtropical Gyre. *Mar Ecol*
562 *Prog Ser* 562:1–18.
- 563 33. Liu H, Nolla HA, Campbell L (1997) *Prochlorococcus* growth rate and contribution to
564 primary production in the equatorial and subtropical North Pacific Ocean. *Aquat Microb*
565 *Ecol* 12(1):39–47.
- 566 34. Kettler GC, et al. (2007) Patterns and implications of gene gain and loss in the evolution
567 of *Prochlorococcus*. *PLoS Genet* 3(12):e231.
- 568 35. Saito MA, et al. (2014) Multiple nutrient stresses at intersecting Pacific Ocean biomes
569 detected by protein biomarkers. *Science (80)* 345(6201):1173–1177.
- 570 36. Mann EL, Chisholm SW (2000) Iron limits the cell division rate of *Prochlorococcus* in
571 the eastern equatorial Pacific. *Limnol Oceanogr* 45(5):1067–1076.
- 572 37. Tagliabue A, et al. (2018) The Role of External Inputs and Internal Cycling in Shaping the
573 Global Ocean Cobalt Distribution: Insights From the First Cobalt Biogeochemical Model.
574 *Global Biogeochem Cycles* 32(4):594–616.
- 575 38. Droop MR (1973) Some thoughts on nutrient limitation in algae. *J Phycol* 9(3):264–272.
- 576 39. Hawco NJ, Saito MA (2018) Competitive inhibition of cobalt uptake by zinc and
577 manganese in a pacific *Prochlorococcus* strain : Insights into metal homeostasis in a
578 streamlined oligotrophic cyanobacterium. *Limnol Oceanogr* 63:2229–2249.
- 579 40. Ho T, et al. (2003) The elemental composition of some marine phytoplankton. *J Phycol*
580 39(6):1145–1159.
- 581 41. Coale KH, Fitzwater SE, Gordon RM, Johnson KS, Barber RT (1996) Control of
582 community growth and export production by upwelled iron in the equatorial Pacific Ocean
583 Kenneth. *Nature* 379(January):1994–1997.
- 584 42. Twining BS, et al. (2011) Metal quotas of plankton in the equatorial Pacific Ocean. *Deep*
585 *Sea Res Part II Top Stud Oceanogr* 58(3–4):325–341.
- 586 43. Cunningham BR, John SG (2017) The effect of iron limitation on cyanobacteria major
587 nutrient and trace element stoichiometry. *Limnol Oceanogr* 62(2):846–858.
- 588 44. Shire DM, Kustka AB (2015) Luxury uptake, iron storage and ferritin abundance in
589 *Prochlorococcus marinus* (*Synechococcales*) strain MED4. *Phycologia* 54(4):398–406.
- 590 45. Raven JA (1990) Predictions of Mn and Fe use efficiencies of phototrophic growth as a
591 function of light availability for growth and of C assimilation pathway. *New Phytol*
592 116(1):1–18.
- 593 46. Raven JA (1988) The iron and molybdenum use efficiencies of plant growth with different
594 energy, carbon and nitrogen sources. *New Phytol* 109(3):279–288.
- 595 47. Goulding CW, Postigo D, Matthews RG (1997) Cobalamin-dependent methionine
596 synthase is a modular protein with distinct regions for binding homocysteine,
597 methyltetrahydrofolate, cobalamin, and adenosylmethionine. *Biochemistry* 36(26):8082–
598 8091.
- 599 48. Licht SS, Lawrence CC, Stubbe J (1999) Class II ribonucleotide reductases catalyze
600 carbon-cobalt bond reformation on every turnover. *J Am Chem Soc* 121(33):7463–7468.
- 601 49. Booker S, Licht S, Broderick J, Stubbe J (1994) Coenzyme B12-Dependent
602 Ribonucleotide Reductase: Evidence for the Participation of Five Cysteine Residues in
603 Ribonucleotide Reduction. *Biochemistry* 33(42):12676–12685.
- 604 50. Goulding CW, Matthews RG (1997) Cobalamin-dependent methionine synthase from
605 *Escherichia coli*: Involvement of zinc in homocysteine activation. *Biochemistry*

- 606 36(50):15749–15757.
- 607 51. Sauter M, Moffatt B, Saechao MC, Wirtz M (2013) Methionine salvage and S -
608 adenosylmethionine : essential links between sulfur, ethylene and polyamine biosynthesis.
609 *Biochem J* 154:145–154.
- 610 52. Moore SJ, et al. (2013) Elucidation of the anaerobic pathway for the corrin component of
611 cobalamin (vitamin B12). *Proc Natl Acad Sci U S A* 110(37):14906–11.
- 612 53. Held NA, McIlvin MR, Moran DM, Laub MT, Saito MA (2019) Unique Patterns and
613 Biogeochemical Relevance of Two-Component Sensing in Marine Bacteria. *MSystems*
614 4(1):e00317-18.
- 615 54. Johnson KS, Stout PM, Berelson WM, Sakamoto-Arnold CM (1988) Cobalt and copper
616 distributions in the waters of Santa Monica Basin, California. *Nature* 332(6164):527–530.
- 617 55. Böning P, et al. (2004) Geochemistry of Peruvian near-surface sediments. *Geochim*
618 *Cosmochim Acta* 68(21):4429–4451.
- 619 56. Hawco NJ, et al. (2018) Cobalt scavenging in the mesopelagic ocean and its influence on
620 global mass balance : Synthesizing water column and sedimentary fluxes. *Mar Chem*
621 201(March 2017):151–166.
- 622 57. Slemons LO, Murray JW, Resing J, Paul B, Dutrieux P (2010) Western Pacific coastal
623 sources of iron, manganese, and aluminum to the Equatorial Undercurrent. *Global*
624 *Biogeochem Cycles* 24(3):n/a-n/a.
- 625 58. Stramma L, Johnson GC, Firing E, Schmidtko S (2010) Eastern Pacific oxygen minimum
626 zones: Supply paths and multidecadal changes. *J Geophys Res* 115(C9):C09011.
- 627 59. Radic A, Lacan F, Murray JW (2011) Iron isotopes in the seawater of the equatorial
628 Pacific Ocean: New constraints for the oceanic iron cycle. *Earth Planet Sci Lett* 306(1–
629 2):1–10.
- 630 60. Mahowald NM, et al. (2005) Atmospheric global dust cycle and iron inputs to the ocean.
631 *Global Biogeochem Cycles* 19(4).
- 632 61. Kwon EY, et al. (2014) Global estimate of submarine groundwater discharge based on an
633 observationally constrained radium isotope model. *Geophys Res Lett* 41(23):8438–8444.
- 634 62. Karstensen J, Stramma L, Visbeck M (2008) Oxygen minimum zones in the eastern
635 tropical Atlantic and Pacific oceans. *Prog Oceanogr* 77(4):331–350.
- 636 63. Ditullio GR, et al. (2003) Phytoplankton assemblage structure and primary productivity
637 along 170 ° W in the South Pacific Ocean. 255:55–80.
- 638 64. Zinser ER, et al. (2007) Influence of light and temperature on *Prochlorococcus* ecotype
639 distributions in the Atlantic Ocean. *Limnol Oceanogr* 52(5):2205–2220.
- 640 65. Schlitzer R, et al. (2018) The GEOTRACES Intermediate Data Product 2017. *Chem Geol*
641 493:210–223.
- 642 66. Saito MA, et al. (2017) The acceleration of dissolved cobalt’ s ecological stoichiometry
643 due to biological uptake, remineralization, and scavenging in the Atlantic Ocean.
644 *Biogeosciences* 14:4637–4662.
- 645 67. Xu Y, Tang D, Shaked Y, Morel FMM (2007) Zinc, cadmium, and cobalt
646 interreplacement and relative use efficiencies in the coccolithophore *Emiliania huxleyi*.
647 *Limnol Oceanogr* 52(5):2294–2305.
- 648 68. John SG, Helgoe J, Townsend E (2018) Biogeochemical cycling of Zn and Cd and their
649 stable isotopes in the Eastern Tropical South Pacific. *Mar Chem* 201:256–262.
- 650 69. Bruland KW (1989) Complexation of zinc by natural organic ligands in the central North
651 Pacific. *Limnol Oceanogr* 34(2):269–285.

- 652 70. Noble AE, Ohnemus DC, Hawco NJ, Lam PJ, Saito MA (2017) Coastal sources, sinks and
653 strong organic complexation of dissolved cobalt within the US North Atlantic
654 GEOTRACES transect GA03. *Biogeosciences* 14(11):2715–2739.
- 655 71. Braakman R, Follows MJ, Chisholm SW (2015) Metabolic evolution and the self-
656 organization of ecosystems. *Proc Natl Acad Sci*. 114(15), 3091-3100.
657 doi:10.1073/pnas.1619573114.
- 658 72. Sperling EA, et al. (2015) Statistical analysis of iron geochemical data suggests limited
659 late Proterozoic oxygenation. *Nature* 523(7561):451–454.
- 660 73. Partensky F, Garczarek L (2010) *Prochlorococcus*: Advantages and Limits of
661 Minimalism. *Ann Rev Mar Sci* 2:305–331.
- 662 74. Biller SJ, Berube PM, Lindell D, Chisholm SW (2015) *Prochlorococcus*: the structure and
663 function of collective diversity. *Nat Rev Micro* 13(1):13–27.
- 664 75. Perez AA, Liu Z, Rodionov DA, Li Z, Bryant DA (2016) Complementation of Cobalamin
665 Auxotrophy in *Synechococcus* sp. Strain PCC 7002 and Validation of a Putative
666 Cobalamin Riboswitch In Vivo. *J Bacteriol* 198(19):2743–2752.
- 667 76. Wilhelm SW, Trick CG (1995) Effects of Vitamin B12 Concentration on Chemostat
668 Cultured *Synechococcus* Sp Strain PCC 7002. *Can J Microbiol* 41(2):145–151.
- 669 77. Kolberg M, Strand KR, Graff P, Andersson KK (2004) Structure, function, and
670 mechanism of ribonucleotide reductases. *Biochim Biophys Acta (BBA)-Proteins
671 Proteomics* 1699(1–2):1–34.
- 672 78. Doxey AC, Kurtz DA, Lynch MDJ, Sauder LA, Neufeld JD (2015) Aquatic metagenomes
673 implicate Thaumarchaeota in global cobalamin production. *ISME J* 9(2):461.
- 674 79. Flombaum P, et al. (2013) Present and future global distributions of the marine
675 Cyanobacteria *Prochlorococcus* and *Synechococcus*. *Proc Natl Acad Sci* 110(24):9824–
676 9829.
- 677 80. Helliwell KE, et al. (2016) Cyanobacteria and Eukaryotic Algae Use Different Chemical
678 Variants of Vitamin B12. *Curr Biol* 26(8):999–1008.
- 679 81. Saito MA, et al. (2011) Iron conservation by reduction of metalloenzyme inventories in
680 the marine diazotroph *Crocospaera watsonii*. *Proc Natl Acad Sci* 108(6):2184–9.
- 681 82. Gouretski V, Koltermann KP (2004) WOCE global hydrographic climatology. *Berichte
682 des BSH* 35:1–52.
- 683
684
685
686
687
688
689
690
691
692
693
694
695

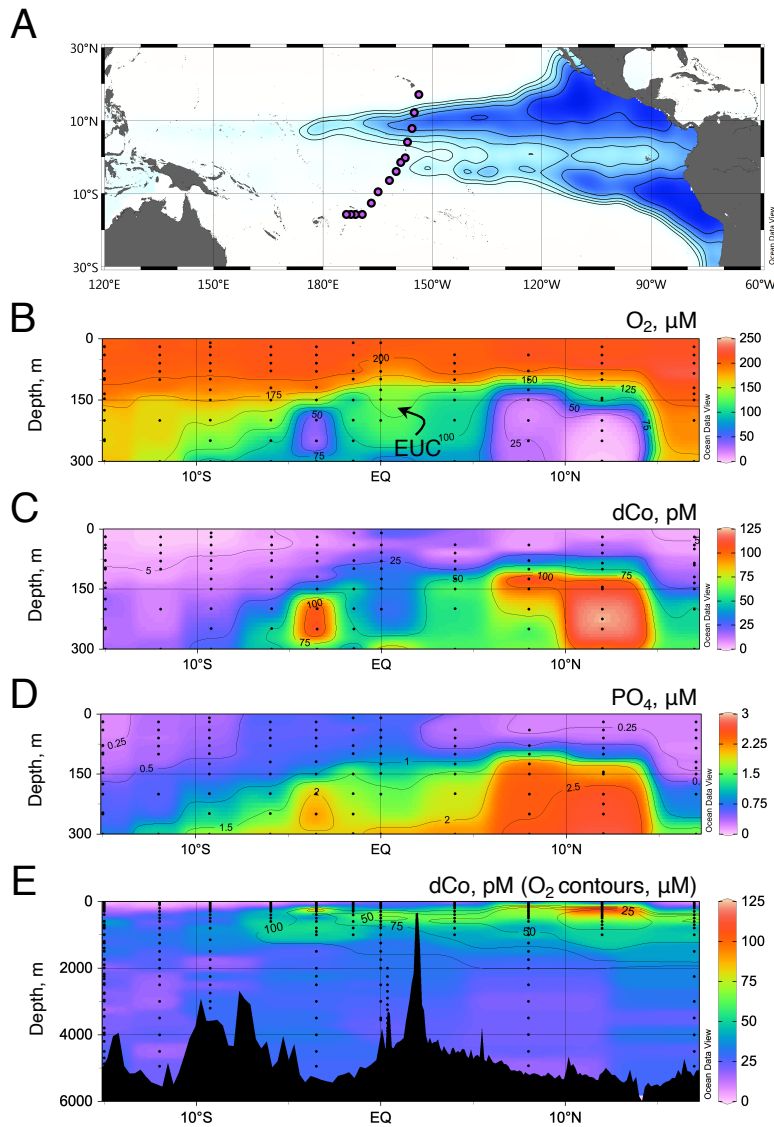
696
697
698
699

Figures



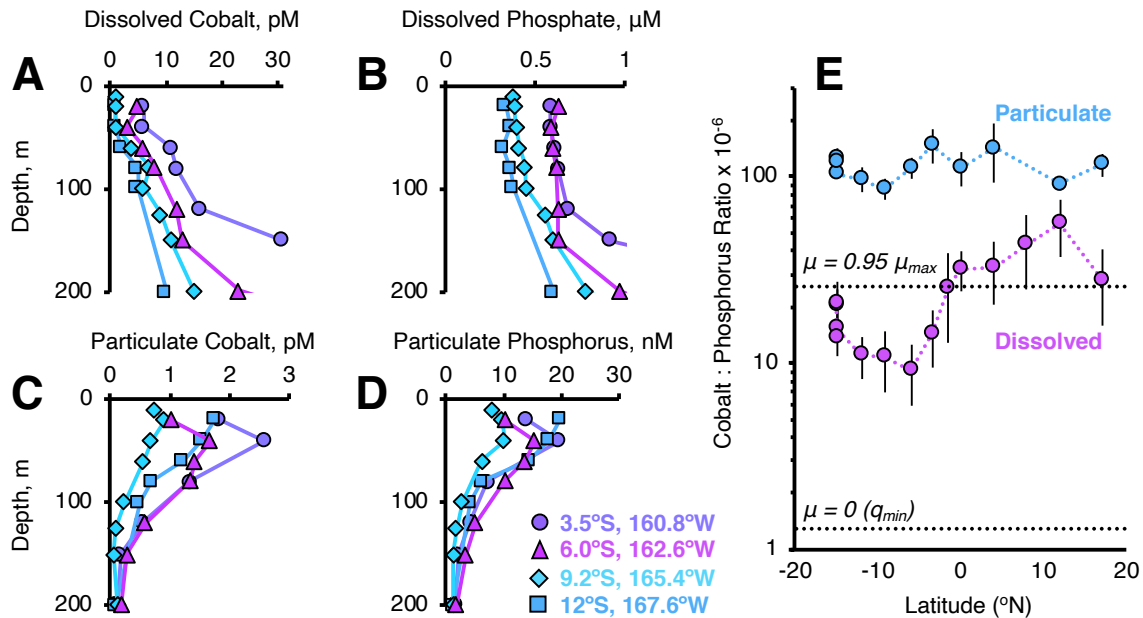
700
701
702
703
704
705
706
707
708
709
710
711
712
713
714

Figure 1. Growth experiments with *Prochlorococcus* MIT9215, originally isolated from the Equatorial Pacific Ocean. A) The exponential growth rate of *Prochlorococcus* MIT9215 as a function of iron (white) and cobalt (blue) concentrations (calculated as the sum of inorganic metal species, Fe' and Co', in equilibrium with EDTA, see methods). B) Dependence of specific growth rate on acquired Fe and Co (i.e. the cell quota), measured by ICPMS. Lines show best fit curves for Eq. 1 and derived values of the minimum cell quota, q_{\min} ($R^2 = 0.96$ for both elements). C) Cell quotas (± 1 SD) of cobalt, the cobalamin-dependent ribonucleotide reductase (NrdJ, blue), and the cobalamin-dependent methionine synthase (MetH, pink). Proteins were quantified by selected reaction monitoring of four tryptic peptides (colored bars) in large volume cultures of cobalt-limited *Prochlorococcus* MIT9215 ($\mu = 0.20$ day⁻¹; see Table S7). Grey lines show predicted levels of these enzymes needed to support maximum growth rates (0.6 day⁻¹) observed in these experiments via use efficiency calculations (Table S4).



715 **Figure 2.** The distribution of dissolved cobalt (dCo) in the Equatorial Pacific Ocean. A) Station
 716 locations (pink circles) from the Metzyme expedition (KM1128) relative to low oxygen water
 717 masses originating on the Peruvian and Mexican margins. Contours mark 25 μM intervals in
 718 dissolved oxygen (O_2) between 25-100 μM at 200m depth from the WOCE gridded atlas (82).
 719 Blue shading highlights low dissolved oxygen. B) A latitudinal section of dissolved oxygen
 720 concentrations from the Metzyme expedition. C) Dissolved cobalt concentrations (operationally
 721 defined as the concentration passing 0.2 μm filter) and D) dissolved phosphate (PO_4) along the
 722 same section. E) The full depth distribution of dissolved cobalt overlain with dissolved oxygen
 723 contours at 25 μM intervals between 0-100 μM O_2 , which highlights their correlation throughout
 724 the water column (Fig. S3).
 725

726
727

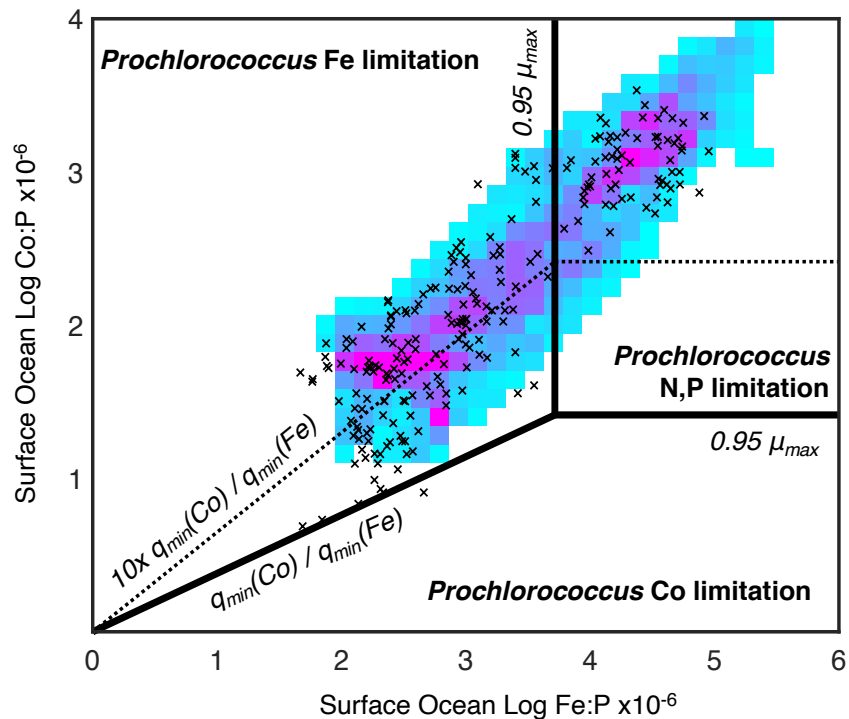


728
729

730 **Figure 3.** Cobalt and phosphate profiles in the South Pacific Ocean from the Metzyme
731 expedition. Removal of dissolved cobalt (A) and dissolved phosphate (B) in the surface ocean is
732 matched by surface maxima of particulate cobalt (C) and particulate phosphorus (D). For A-D,
733 colors and shapes indicate station locations. E) The ratio of cobalt to phosphorus in the euphotic
734 zone (0-100 m) along the Metzyme transect in both dissolved (pink) and particulate (blue)
735 phases. Dotted black lines indicate the Co:P composition of cobalt-limited *Prochlorococcus*
736 MIT9215 biomass at threshold growth rates of 0 and 95% μ_{max} via Eq. 1 (see Table S1).

737
738
739
740
741
742
743
744
745
746
747
748
749
750
751
752

753
754



755
756

757 **Figure 4.** Global analysis of cobalt depletion in the marine habitat of *Prochlorococcus*, defined
758 as waters with temperature >12°C. Colors represent the relative pixel density of modelled
759 stoichiometry of total Co:PO₄ and Fe:PO₄ (the sum of dissolved and particulate phases) in the
760 surface ocean, with pink colors indicating a large number of pixels (i.e. model grid cells).
761 Crosses indicate measurements of dissolved Co, Fe, and PO₄ from the GEOTRACES
762 Intermediate Data Product 2017 (65) from the surface mixed layer (0–30 m). Minimum Co and
763 Fe requirements of *Prochlorococcus* MIT9215 are used to define growth limitation domains for
764 Co and Fe (solid black lines). Dashed lines mark the shift in nutrient limitation domains if cobalt
765 requirements increased by 10-fold (a Co:P ratio of 260 x10⁻⁶ at 95% μ_{max}), which corresponds to
766 Co:P ratios of *Emiliana huxleyi* cultures grown in low Zn media (67).

767
768
769

Supplemental Information for

Minimal cobalt metabolism in the marine cyanobacterium Prochlorococcus

Nicholas J. Hawco^{1,2,†,*}, Matthew M. McIlvin¹, Randelle M. Bundy^{1,3}, Alessandro Tagliabue⁴, Tyler J. Goepfert^{1,5}, Dawn M. Moran¹, Luis Valentin-Alvarado^{1,6}, Giacomo R. DiTullio⁷ and Mak A. Saito^{1*}

¹ Department of Marine Chemistry and Geochemistry, Woods Hole Oceanographic Institution, Woods Hole MA, USA

² Department of Earth Sciences, University of Southern California, Los Angeles CA, USA

³ School of Oceanography, University of Washington, Seattle WA, USA

⁴ Department of Earth, Ocean and Ecological Sciences, University of Liverpool, Liverpool UK

⁵ School of Earth and Space Exploration, Arizona State University, Tempe AZ, USA

⁶ Department of Plant and Microbial Biology, University of California at Berkeley, Berkeley CA USA

⁷ Hollings Marine Lab, College of Charleston, Charleston SC, USA

†Present address: Department of Oceanography, University of Hawaii at Manoa, Honolulu HI

* Corresponding Authors. Contact: hawco@hawaii.edu, 1000 Pope Road, 808-956-2613; msaito@whoi.edu, 266 Woods Hole Road MS#51, 508-289-2393.

This PDF file includes:

1. Supplemental Methods
2. Supplemental References
3. Supplemental Figures S1- S11
4. Supplemental Tables S1 to S8

1. Supplemental methods

Culturing procedures

Prochlorococcus strain MIT9215 was originally isolated from the Equatorial Pacific in Oct. 1992 (1). Axenic cultures were provided by the Chisholm lab at MIT and grown at 27°C in a custom incubator under a 14:10 light:dark cycle at a peak light intensity of 75 $\mu\text{mol photon m}^{-2} \text{ s}^{-1}$. For all experiments, cells were inoculated at 1% media volume or lower from cultures in mid-late exponential phase. Growth was monitored by *in vivo* chlorophyll fluorescence. Cultures were grown in a modified ProTM media (2) where concentrations of inorganic metal species (denoted as metal') are stabilized by equilibrium with ethylenediamine tetraacetic acid (EDTA) (3). At an EDTA concentration of 11.7 μM , the ratio of Fe' to total iron is $10^{-1.94}$ and the ratio of Co' to total cobalt is $10^{-2.81}$ (4). Background iron and cobalt concentrations were determined to be 0.3 and 0.01 nM, respectively. For all experiments, Fe' (maximum 135 pM) was below Fe hydroxide solubility thresholds (~ 500 pM (5)).

Cells were harvested by centrifugation, digested in 5% nitric acid, and analyzed by ICP-MS (4). Samples were corrected for matrix effects using a 1ppb In internal standard and calibrated relative to a 1-100 ppb standard curve made from a certified multielement standard (Spex Certiprep). Duplicate analyses of cell digests agreed within 5% for both Co and Fe, except at Co levels below 30 atoms per cell which agreed to $\sim 20\%$. Process blanks were subtracted from measured concentrations. The mean blank for this dataset was 0.022 pmol for Co and 12.4 pmol for Fe. Detection limits (as 3-times the standard deviation of the blank, $n=12$) were 0.044 pmol for Co and 30 pmol for Fe. Phosphorus concentrations were also measured by ICP-MS and calibrated to a separate standard curve ranging from 100–1500 ppb sodium phosphate, which was cross-calibrated to a certified 1 ppm P standard (Alfa Aesar Specpure). Metal and P concentrations in digestions were scaled to original culture volume and divided by cell number to derive per cell quotas. Harvested cells were not washed with chelating solutions (6) to remove extracellularly-bound metals, but low Fe' concentrations used in these experiments suggest minimal Fe precipitation onto cell surfaces, consistent with laboratory validation studies (7).

For all samples where quotas were measured, cell number was determined by flow cytometry on a Guava EasyCyte HT instrument with InCyte 3.1 software. Cultures were serially diluted in filtered oligotrophic seawater and counted using a red fluorescence gate until 5000 events were recorded. This instrument was calibrated monthly with beads. Dilutions with cell concentrations in the range of $0.5\text{--}2 \times 10^5$ cells per ml were used to calculate original cell number. No difference was observed in cell number of nutrient replete, exponential phase cultures preserved with 5% paraformaldehyde, flash frozen in liquid nitrogen and stored at -80 °C (cobalt-limitation series, 5.3×10^7 cells/ml) versus cells that were frozen directly at -80 °C (iron-limitation series, 5.5×10^7 cells/ml). Cell density of media supernatant following centrifugation was also measured to evaluate harvesting efficiency by this method. In general, harvesting efficiency by centrifugation was $>95\%$, except at low cell densities where harvesting efficiency was still $>80\%$. Agreement between cellular P quotas ($1.1 \pm 0.4 \times 10^7$ atoms per cell, Table S2) and literature data for this strain ($0.4\text{--}0.7 \times 10^7$ atoms per cell (8)) and *Prochlorococcus* Med4 ($0.2\text{--}2 \times 10^7$ atoms per cell (9)), indicate that ICPMS and flow cytometry determinations are robust. The 1.7 M bp genome of *Prochlorococcus* MIT9215 alone accounts for 0.3×10^7 P atoms per cell, a considerable fraction of the cellular P quota. Metal:C ratios were

estimated as the mean of two approaches: 1) a conversion of metal cell⁻¹ quotas using a C cell⁻¹ quota ($1.85 \pm 0.23 \times 10^9$ C atoms cell⁻¹) and 2) the product of the metal:P ratio and the P:C ratio (325 ± 74 mol:mol). Both conversion factors reflect published measurements of the *Prochlorococcus* MIT9215 strain (8) and uncertainties are propagated throughout.

Additional culturing protocols, plasticware cleaning procedures, media preparation, and measurement of growth rates and cell quotas are identical to those described by Hawco and Saito (2018) and methodological details can be found there (4). All curve fitting was performed with using least-squares routines in Sigma Plot 12.

Protein Extraction and Global Proteomic Analysis

Soluble proteins were extracted from cell pellets and digested using a detergent-free method (10). Biomass was resuspended in 100 mM ammonium bicarbonate and sonicated on ice at 70% duty for two 4-minute intervals and then centrifuged at 14,000 rpm for 20 minutes at 4°C. 200 µl of supernatant was precipitated in 800 µl acetone at -20°C for several days. The supernatant solution was removed after spinning at 14,000 rpm at 4°C and precipitated proteins were dried on a speed-vac (Thermo) for several minutes.

Extracted protein was resuspended with 125 µl of 6M urea in 100 mM ammonium bicarbonate and heated to 95°C to dissolve. 100 µl of this sample was then incubated with 5 µl of 200 mM dithiothreitol (DTT) for 1 hour at 56°C, 20 µl of 200 mM iodoacetamide for 1 hour at room temperature, and finally for 1 hour at room temperature with an additional 20 µl of 200 mM DTT. Samples were diluted to 1 ml in 100 mM ammonium bicarbonate and trypsin (Promega Gold) was added at a 1:50 ratio to total protein, quantified by a detergent compatible (DC) colorimetric assay (Bio-Rad) at 750 nm on a UV-Vis spectrophotometer (Shimadzu). Samples were digested overnight at 37°C. Peptides were concentrated by speed-vac and then diluted with an LC-MS buffer containing 98% water, 2% acetonitrile, and 0.1% formic acid to a final protein concentration of 0.1 µg/µl.

Global proteome composition was analyzed by liquid chromatography mass spectrometry (LC-MS) following previously described procedures (11). Protein extracts were analyzed in duplicate. Raw mass spectrometry files were searched using *Prochlorococcus* MIT9215 genome (downloaded from NCBI) and scored through the Sequest algorithm using Proteome Discoverer software (Thermo). Mass tolerance settings of 10 ppm for parent ions and 0.02 Da for fragments were used with fixed cysteine carbamidomethylation (+57), variable methionine oxidation (+16), and a maximum of 2 missed trypsin cleavages. Processed data were assembled and spectra were counted using Scaffold 4.7.3 with 95% minimum peptide thresholds and 99.9% minimum protein thresholds applied. False discovery rates for the cobalt gradient experiment (10, 3, 1 and 0.6 nM Co) was calculated to be 0.2% for decoy peptides and 5.5% for decoy proteins.

A Fisher's Exact test was applied to 584 detected proteins to compare spectral counts between cobalt-limited samples (0.6 and 1 nM Co) and cobalt replete samples (3 and 10 nM Co) with significance being determined at $p < 0.01$. Prior to plotting, this dataset was reduced by eliminating proteins that were not identified in each of the 4 samples (2 treatments with 2 technical replicates) within the cobalt-limited or cobalt-replete groups. Figure S2B shows the 121 proteins that meet these criteria, 20 of which were significantly more abundant and 14 of which were significant less abundant (Table S9), with error bars in Fig. S2B reflecting the standard deviation between 4 samples.

Quantitative Protein Measurements of NrdJ and MetH

Due to their low abundance, neither NrdJ nor MetH were detected using the strict settings needed to interpret global proteomes. Instead, *Prochlorococcus* MIT9215 methionine synthase (*metH*, P9215_10151) and ribonucleotide reductase (*nrdJ*, 9215_07641) peptides were quantified by selected reaction monitoring (SRM) by targeted liquid chromatography mass spectrometry, which required additional *Prochlorococcus* biomass and the generation of isotopically labeled standards.

Large volume cultures of cobalt-limited *Prochlorococcus* MIT9215 cultures (non-axenic) were grown in 8 L polycarbonate carboys and sampled over several days during exponential growth. Four 30 mL aliquots were taken at the start of exponential phase and grown in 28 mL polycarbonate tubes alongside larger carboys to measure growth rate under similar light and media conditions. Growth rates increased when additional cobalt was added to two of these aliquots to validate that cells were indeed limited by cobalt.

Chlorophyll fluorescence of aliquots collected in 8 L carboys during sample harvesting agreed with levels in 28 mL cultures, suggesting that growth in both bottles grew similarly over these short timescales (<7 days). Biomass for metal and protein measurements was harvested simultaneously. In addition to measuring cellular cobalt quotas in these samples (described above), the cobalt content of the acetone supernatant during protein extraction was measured after evaporating to dryness by speed-vac and digesting in 5% nitric acid. The cobalt concentration in these aliquots indicated that between 30–70% of the cobalt quota was released during sonication and, by inference, a similar percentage of cobalt-bearing proteins. It is likely that a greater fraction of NrdJ and MetH were extracted. Biochemical studies with homologous enzymes have demonstrated that both proteins are soluble in aqueous solution, suggesting that the protein extraction procedure employed is able to recover these enzymes (12, 13). Because detergent-free protein extractions discriminate against lipophilic proteins associated with plasma or photosynthetic membranes, cobalt bound to these proteins may account for the ‘missing’ cobalt quota. This may include cobalt-bearing intermediates of the B₁₂ biosynthetic pathway, which is probably membrane bound (14). However, the higher reagent blanks associated with measuring cobalt in protein extracts compared to acid digestions make the former determinations more uncertain.

Isotope labeled peptide standards were generated by overexpression of a pET30-a plasmid with sequences for *Prochlorococcus nrdJ*, *metH* and horse myoglobin peptides (Fig. S9) in competent *E. coli* cells (Novagen Tuner(DE3) pLysS). Individual colonies were selected and grown in 10 mL of ¹⁵N-labeled media (Cambridge Isotope Laboratories Bioexpress Cell Growth Media U-15N, 98%) amended with 100 mg L⁻¹ kanamycin, overnight at 34°C. Afterwards, 100 µL of cells were inoculated into 10 mL of ¹⁵N labeled media and induced with 1 mM IPTG after 3 hours at 34°C. Induced cells were harvested after 24 hours at 20°C by centrifugation at 6500 g for 20 min at 4°C and frozen at -20°C. Cell pellets were then lysed with 1 mL soluble lysis reagent (Novagen Bug Buster protein extraction reagent amended with 25 units of Benzonase Nuclease) and centrifuged at 6500 g for 20 min at 4°C, after which the supernatant solution was decanted from the pellet of inclusion bodies. Inclusion bodies were dissolved in 6M urea and digested with trypsin according to the above protocol. Labeled peptides were analyzed by LC-MS to ensure complete trypsin digestion and the absence of detectible peptides with natural isotope abundance. A manuscript describing this method in detail is forthcoming (McIlvin and Saito, *in prep.*)

Labeled peptides were calibrated relative to commercial horse myoglobin (Fischer), which was resuspended in ammonium bicarbonate to 100 nM and digested overnight with 6 µg trypsin at room temperature. Addition of a known quantity of commercial horse myoglobin peptides (unlabeled) was used to quantify the concentration of ¹⁵N-labeled myoglobin peptides that were overexpressed in *E. coli* (Table S6). Because ¹⁵N-labeled *Prochlorococcus* peptides and ¹⁵N-labeled myoglobin peptides were cloned from a single sequence, the measured concentration of ¹⁵N-labeled myoglobin peptides is equal to the concentration of ¹⁵N-labeled *Prochlorococcus* NrdJ and MetH peptides. Digested, ¹⁵N-labeled peptides were added to digested *Prochlorococcus* peptides (0.1 µg/µl total protein) to a final concentration of 3.3 fmol/µl of labeled peptide. 10 µl of sample was injected onto a 5 µm C18 peptide trap connected to a 3 µm C18 column. Peptides were separated with a Microhm Advance liquid chromatography system over a gradient of 0-95% acetonitrile over a 40 minute window. This gradient increased linearly from 2 to 40% over the first 30 minutes and increased to 95% acetonitrile over the next 5 minutes. Secondary mass spectra (MS²) were collected with a Q-Exactive mass spectrometer (Thermo) using an inclusion list containing both heavy and light peptide masses. The ratio of labeled and unlabeled peptides was then used to determine the concentration of NrdJ and MetH in protein digests (fmol/µg protein digested, Table S7, Figs. S10, S11). Skyline targeted proteomics software (<https://skyline.ms/project/home/begin.view?>) was used to process MS² spectra and calculate peptide ratios.

Peptide concentrations were corrected for dilution and sample splitting during protein digestion to arrive at a cellular quota. We excluded two of the six peptides that were cloned for each enzyme due to anomalously low sensitivity of labeled standards or poor peak resolution in samples. The concentration of remaining peptides agreed to a reasonable extent (~20%) with relative abundance trends between samples being more consistent.

Following measurement of these proteins in large volume *Prochlorococcus* MIT9215 cultures, NrdJ and MetH abundance was determined in protein extracts from the cobalt-gradient experiment (10, 3, 1, 0.6 nM Co). The relative abundance of NrdJ and MetH in these samples was quantified (e.g. Fig. S2A) but could not be reliably related to a cellular quota due to low extraction/retention efficiency at low protein concentration in these samples. The ratio of NrdJ to MetH peptides was similar between large volume cobalt-limited cultures (2.3) and cobalt-limited cultures from the Co gradient experiment (2.9), suggesting that relative abundance measurements for this dataset are robust (Table S7)

Dissolved and particulate cobalt distributions in the Equatorial Pacific Ocean.

The Metzyme cruise (KM1128) was conducted during October 2011, between Honolulu, Hawai'i and Apia, Western Samoa. The transect followed a North-South line at 155 °W to the equator and proceeded to the southwest to 15°S, 170°W (Fig. 2A). Trace metal clean sampling procedures and nutrient analyses have been fully described by Saito et al., 2014 (15). Samples for dissolved cobalt determinations were 0.2 µm filtered with 47 mm Supor filters (saved for particulate analyses) in a clean space maintained by HEPA air filtration. Filtered samples were stored in 60 ml acid-clean polyethylene bottles at 4 °C and preserved with metal-free gas absorbing satchels (Mitsubishi Gas and Chemical) in heat sealed bags, with 3 satchels and 6 samples per bag.

Dissolved cobalt concentrations were determined by cathodic stripping voltammetry (CSV) using dimethylglyoxime (DMG) as a competing ligand following UV-oxidation to destroy organic cobalt ligands (16). Cobalt profiles from stations 1 (17°N), 3 (8°N), and 5 (0°N)

were published previously (15). All other samples were measured concurrently with dissolved cobalt for samples for that GEOTRACES GP16 dataset, following identical analytical procedures (17). During this time, stations 1, 3, and 5 were re-run and agreed with published values for these samples, except for samples from the oxygen minimum zone in Station 3 (8°N), where some cobalt (~20 pM) seemed to have been lost over ~2 years since removal from O₂-free bags, an effect that has been documented in the oxygen minimum zone of the North Atlantic (18). A blank of 4.6 pM ± 0.7 pM Co was determined from 19 analyses of Chelex-100 treated, UV oxidized seawater (16). This blank reflects cobalt added from reagents and other sources during analyses. The detection limit of this dataset, calculated as 3-times the standard deviation of the blank, was 2.1 pM. Ocean sections in Figure 2 made using Ocean Data View version 4.7.10 (Schlitzer, R., <https://odv.awi.de>).

Particulate cobalt and particulate phosphate were measured on 0.2 µm Supor filters (47 mm) used for filtering seawater collected in 8 L X-Niskin bottles (15). Filters returned to the lab frozen and were digested in 50% trace metal grade nitric acid with 1ppb Indium at 90 °C for 3 hours, diluted to 5% nitric acid with ultrapure water (Milli-Q), and analyzed on an Element 2 mass spectrometer in the WHOI ICP-MS facility. Indium was used as an internal standard to correct for sample injection and dilution. The instrument was calibrated using external standards diluted from certified standards (SPEX Certiprep) and filter blanks were subtracted from measured values.

Analyses with the PISCES Cobalt Biogeochemical Model

Field observations of seawater Co:P stoichiometry were extrapolated to the global ocean using a recently developed biogeochemical model of the marine cobalt cycle (19). This model operates within the PISCES biogeochemical framework (20). All cobalt-related parametrizations are added without feedback to the base model (i.e. no feedbacks on phytoplankton growth, macronutrient uptake etc.). The cobalt model was rerun following an update to the underlying biogeochemical descriptions of the PISCES model to incorporate new descriptions of POC flux and remineralization (21). Despite no new changes to Co-related parametrizations, the new simulations represent an improved fit to observations compared to the published model and produce lower cobalt concentrations in the surface of the South Pacific Ocean, consistent with measured values.

To determine the total metal:phosphorus ratio for surface ocean grid cells, cobalt, iron and P pools across dissolved and particulate phases were summed. Grid cells with mean annual temperatures below 12°C were excluded from analysis because culture and field evidence suggest *Prochlorococcus* is not found in these waters (22). Model data are plotted in Figs. 4, S5, S6, and S8.

The fidelity of modelled Co:P and Fe:P ratios was assessed by comparison to high-quality cobalt, iron and phosphate measurements compiled in the GEOTRACES Intermediate Data Product 2017 (23). Co-located Fe, Co, and P concentrations from the upper 30 m of the ocean were extracted (n = 231). This depth range was chosen to maximize the number of samples while avoiding upwelling signals derived from the nutricline. Of these measurements, 33 had Co:PO₄ ratios below 26 µmol:µmol, mostly from the GP16 transect in the Eastern Tropical South Pacific (17). Because of significant uncertainty in these parameters at very low concentrations, minimum concentrations of 3 pM Co, 50 pM Fe, and 20 nM P were imposed. Note that because this database only includes PO₄ measurements, this threshold helps to acknowledge the presence of bioavailable dissolved organic phosphorus that supports

phytoplankton growth at extremely low PO₄. The choice of these lower limits does not have a meaningful impact on the distribution of data in Figure 4.

4. Supplemental references

1. Moore LR, Chisholm SW (1999) Photophysiology of the marine cyanobacterium *Prochlorococcus*: ecotypic differences among cultured isolates. *Limnol Oceanogr* 44(3):628–638.
2. Moore LR, et al. (2007) Culturing the marine cyanobacterium *Prochlorococcus*. *Limnol Oceanogr Methods* 5:353–362.
3. Sunda W, Price N, Morel F (2005) Trace metal ion buffers and their use in culture studies. *Algal Culturing Techniques* (Academic Press), pp 35–63.
4. Hawco NJ, Saito MA (2018) Competitive inhibition of cobalt uptake by zinc and manganese in a pacific *Prochlorococcus* strain : Insights into metal homeostasis in a streamlined oligotrophic cyanobacterium. *Limnol Oceanogr* 63:2229–2249.
5. Sunda WG, Huntsman SA (1997) Interrelated influence of iron, light and cell size on marine phytoplankton growth. *Nature* 390(6658):389–392.
6. Tang D, Morel FMM (2006) Distinguishing between cellular and Fe-oxide-associated trace elements in phytoplankton. *Mar Chem* 98(1):18–30.
7. Ho T, et al. (2003) The elemental composition of some marine phytoplankton. *J Phycol* 39(6):1145–1159.
8. Martiny AC, Ma L, Mougnot C, Chandler JW, Zinser ER (2016) Interactions between thermal acclimation, growth rate, and phylogeny influence *Prochlorococcus* elemental stoichiometry. *PLoS One* 11(12):e0168291.
9. Bertilsson S, Berglund O, Karl DM, Chisholm SW (2003) Elemental composition of marine *Prochlorococcus* and *Synechococcus*: Implications for the ecological stoichiometry of the sea. *Limnol Oceanogr* 48(5):1721–1731.
10. Cox AD, Saito MA (2013) Proteomic responses of oceanic *Synechococcus* WH8102 to phosphate and zinc scarcity and cadmium additions. *Front Microbiol* 4(DEC):1–17.
11. Mackey KRM, et al. (2015) Divergent responses of Atlantic coastal and oceanic *Synechococcus* to iron limitation. *Proc Natl Acad Sci* 112(32):9944–9949.
12. Goulding CW, Matthews RG (1997) Cobalamin-dependent methionine synthase from *Escherichia coli*: Involvement of zinc in homocysteine activation. *Biochemistry* 36(50):15749–15757.
13. Licht SS, Lawrence CC, Stubbe J (1999) Class II ribonucleotide reductases catalyze carbon-cobalt bond reformation on every turnover. *J Am Chem Soc* 121(33):7463–7468.
14. Patterson CJ, et al. (2013) Co(ii)-detection does not follow K_{co(ii)} gradient: channelling in Co(ii)-sensing. *Metallomics* 5(4):352–362.
15. Saito MA, et al. (2014) Multiple nutrient stresses at intersecting Pacific Ocean biomes detected by protein biomarkers. *Science* (80) 345(6201):1173–1177.
16. Saito MA, Moffett JW (2001) Complexation of cobalt by natural organic ligands in the Sargasso Sea as determined by a new high-sensitivity electrochemical cobalt speciation method suitable for open ocean work. *Mar Chem* 75(1–2):49–68.
17. Hawco NJ, Ohnemus DC, Resing JA, Twining BS, Saito MA (2016) A cobalt plume in the oxygen minimum zone of the Eastern Tropical South Pacific. *Biogeosciences*

- 13:5697–5717.
18. Noble AE, Ohnemus DC, Hawco NJ, Lam PJ, Saito MA (2017) Coastal sources, sinks and strong organic complexation of dissolved cobalt within the US North Atlantic GEOTRACES transect GA03. *Biogeosciences* 14(11):2715–2739.
 19. Tagliabue A, et al. (2018) The Role of External Inputs and Internal Cycling in Shaping the Global Ocean Cobalt Distribution: Insights From the First Cobalt Biogeochemical Model. *Global Biogeochem Cycles* 32(4):594–616.
 20. Aumont O, Ethe C, Tagliabue A, Bopp L, Gehlen M (2015) PISCES-v2 : an ocean biogeochemical model for carbon and ecosystem studies. *Geosci Model Dev* 8:2465–2513.
 21. Aumont O, et al. (2017) Variable reactivity of particulate organic matter in a global ocean biogeochemical model. *Biogeosciences* 14(9):2321–2341.
 22. Zinser ER, et al. (2007) Influence of light and temperature on *Prochlorococcus* ecotype distributions in the Atlantic Ocean. *Limnol Oceanogr* 52(5):2205–2220.
 23. Schlitzer R, et al. (2018) The GEOTRACES Intermediate Data Product 2017. *Chem Geol* 493:210–223.
 24. Rii YM, Karl DM, Church MJ (2016) Temporal and vertical variability in picophytoplankton primary productivity in the North Pacific Subtropical Gyre. *Mar Ecol Prog Ser* 562:1–18.
 25. Malmstrom RR, et al. (2010) Temporal dynamics of *Prochlorococcus* ecotypes in the Atlantic and Pacific oceans. *ISME J* 4(10):1252.
 26. Xu Y, Tang D, Shaked Y, Morel FMM (2007) Zinc, cadmium, and cobalt interreplacement and relative use efficiencies in the coccolithophore *Emiliania huxleyi*. *Limnol Oceanogr* 52(5):2294–2305.
 27. Webb EA, Moffett JW, Waterbury JB (2001) Iron stress in open-ocean cyanobacteria (*Synechococcus*, *Trichodesmium*, and *Crocospaera* spp.): Identification of the idia protein. *Appl Environ Microbiol* 67(12):5444–5452.
 28. Raven JA (1990) Predictions of Mn and Fe use efficiencies of phototrophic growth as a function of light availability for growth and of C assimilation pathway. *New Phytol* 116(1):1–18.
 29. Raven JA (1988) The iron and molybdenum use efficiencies of plant growth with different energy, carbon and nitrogen sources. *New Phytol* 109(3):279–288.
 30. Sintchak MD, Arjara G, Kellogg BA, Stubbe J, Drennan CL (2002) The crystal structure of class II ribonucleotide reductase reveals how an allosterically regulated monomer mimics a dimer. *Nat Struct Mol Biol* 9(4):293.
 31. Kettler GC, et al. (2007) Patterns and implications of gene gain and loss in the evolution of *Prochlorococcus*. *PLoS Genet* 3(12):e231.
 32. Drennan CL, Huang S, Drummond JT, Matthews RG, Ludwig ML (1994) How a protein binds B₁₂: a 3.0 Å X-ray structure of B₁₂-binding domains of methionine synthase. *Science* 266(5191):1669–74.
 33. Banerjee R V, Frasca V, Ballou DP, Matthews RG (1990) Participation of cob(I) alamin in the reaction catalyzed by methionine synthase from *Escherichia coli*: a steady-state and rapid reaction kinetic analysis. *Biochemistry* 29(50):11101–9.
 34. Heldal M, Scanlan DJ, Norland S, Thingstad F, Mann NH (2003) Elemental composition of single cells of various strains of marine *Prochlorococcus* and *Synechococcus* using X-ray microanalysis. *Limnol Oceanogr* 48(5):1732–1743.

3. Supplemental figures

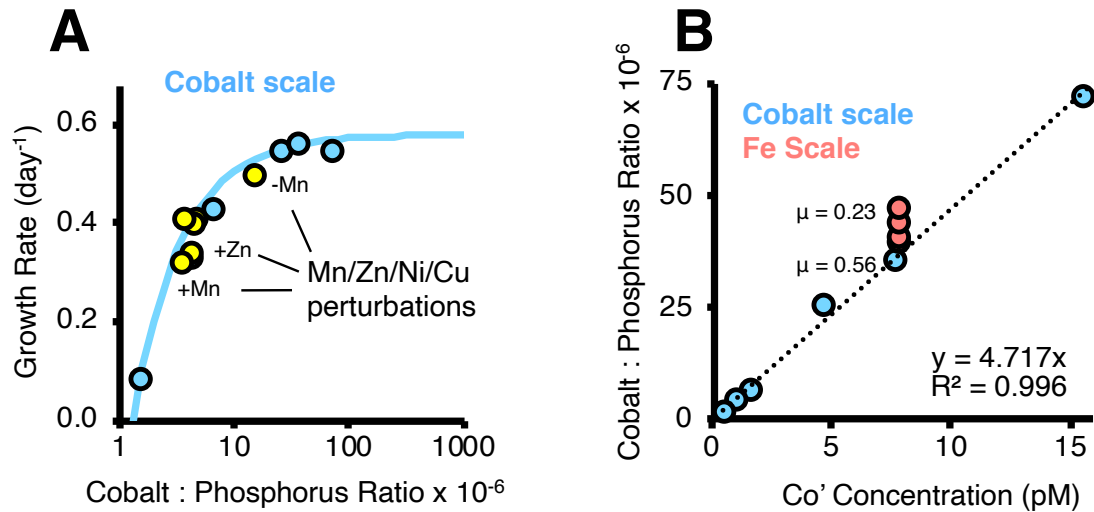


Figure S1. A) Growth of *Prochlorococcus* MIT9215 cultures as a function of the cellular Co:P ratio. Blue points show results from experiments where Co' concentration was varied but all other metals were held constant. The blue line shows a fit of the Droop Curve for these data ($R^2 = 0.96$, see Table S1). Yellow circles show results from metal perturbation experiments under a constant, limiting concentration of Co' (4). Media with additional Mn and Zn depressed growth rates while media with less added Mn increased growth rates. Additional treatments (+Ni, -Ni, +Cu) did not strongly affect growth and are unlabeled. Note the similarity between Co:P ratio and growth rate in both sets of experiments implies that Zn/Mn effects are primarily associated with competitive inhibition at the transporter site and not intracellular toxicity (see Hawco and Saito 2018). B) Evidence for additional Co uptake by *Prochlorococcus* under Fe limitation. Blue circles show linear relationship between cellular Co:P and the media Co' concentration ($R^2 > 0.99$). Red circles show Co:P ratio as cells become more Fe limited. Note that Co' in these experiments is held constant.

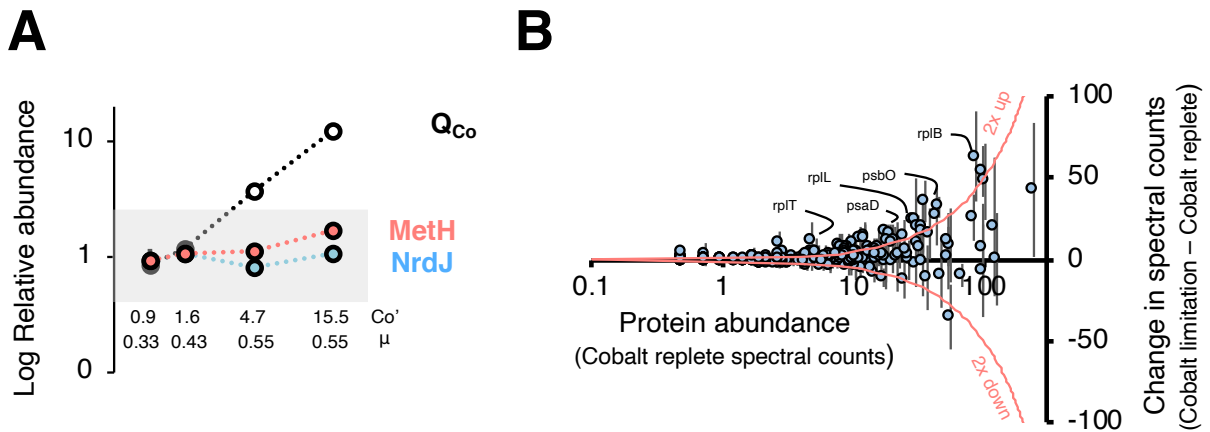


Figure S2. Proteomic measurements of cobalt-limited metabolism of *Prochlorococcus* MIT9215. A) Relative abundance of cobalamin-dependent ribonucleotide reductase (NrdJ, blue circles) and cobalamin-dependent methionine synthase (MetH, red circles) as a function of growth rate and cobalt concentration, determined by selected reaction monitoring of four tryptic peptides. White circles show relative change in the cellular cobalt quota, Q_{Co} , which has a maximum value of 780 atoms per cell. B) Whole cell proteomes under cobalt limitation. Vertical axis reflects the difference in assigned spectral counts in cobalt-limited samples (0.3 and 1.6 pM Co^{2+}) relative to cobalt-replete samples (4.7 and 15.5 pM Co^{2+}), with positive values reflecting upregulation under cobalt limitation. Red lines follow trajectories of a two-fold up- or down-regulation. Select up-regulated proteins are annotated (see Table S8 for a complete list).

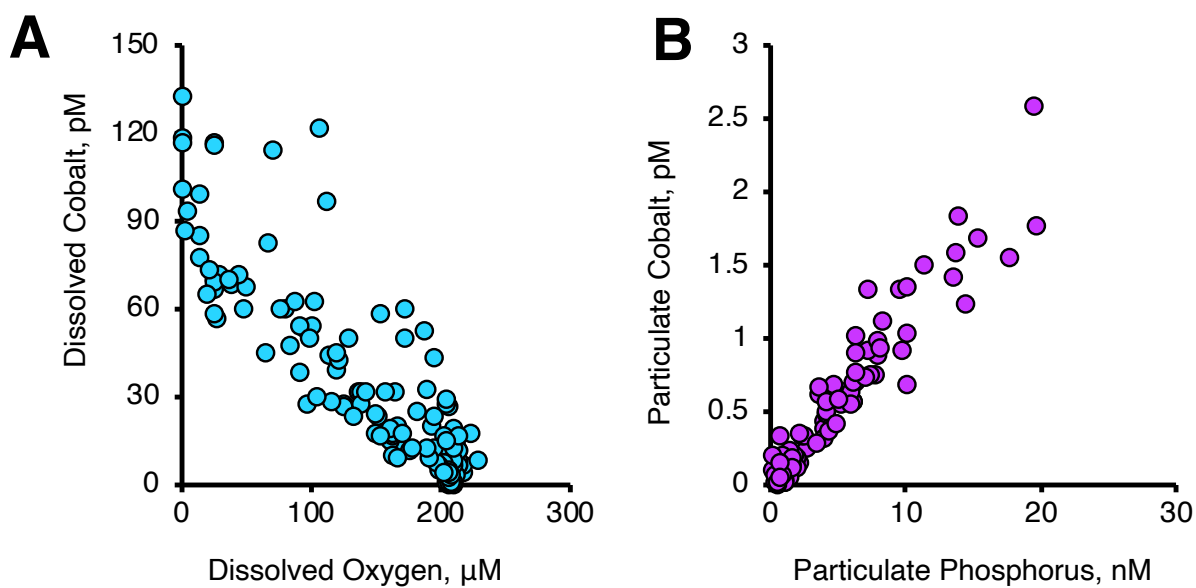


Figure S3. A) Relationship between dissolved cobalt and dissolved oxygen concentration for samples from 0–500 m from the Metzyme cruise (KM1128). B) Relationship between particulate cobalt and particulate phosphorus, also from samples between 0–500 m (note samples with elevated concentrations of both elements are all from the upper 100 m). The slope of this relationship is 110×10^{-6} ($R^2 = 0.92$).

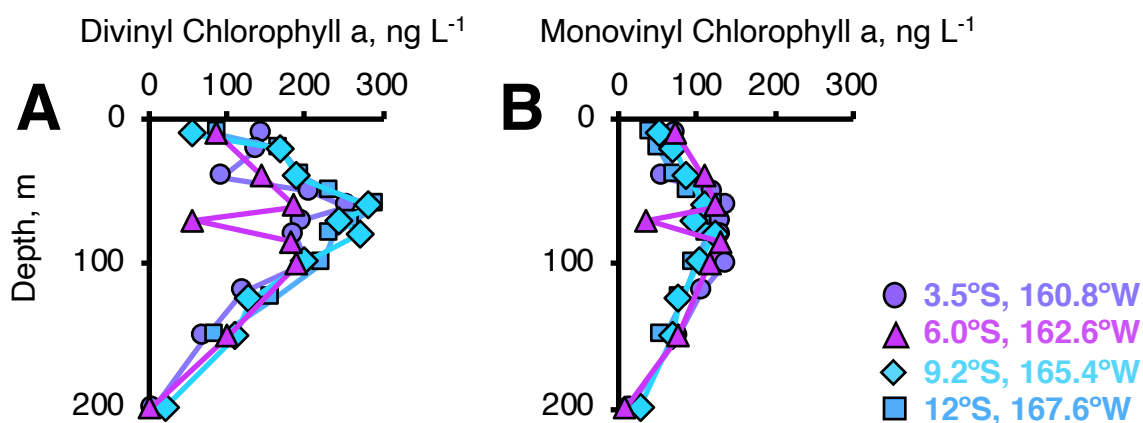


Figure S4. Profiles of divinyl chlorophyll a (A) and monovinyl chlorophyll (B) during the Metzyme cruise, October 2011 (KM1128) for stations in the South Pacific. The divinyl chlorophyll *a* pigment is unique to *Prochlorococcus* and exceeds monovinyl chlorophyll *a* (synthesized by other phytoplankton) for each of these stations. Symbols and color scheme match those in Figure 3A-D. Note that the increase of both chlorophyll types with depth represents an increase in chlorophyll:C ratios (as a response to decreasing light), and not an increase in biomass. Studies in the North Pacific subtropical gyre have emphasized that *Prochlorococcus* growth rates are fastest in the mixed layer (24), where HLII *Prochlorococcus* ecotypes are most abundant (25).

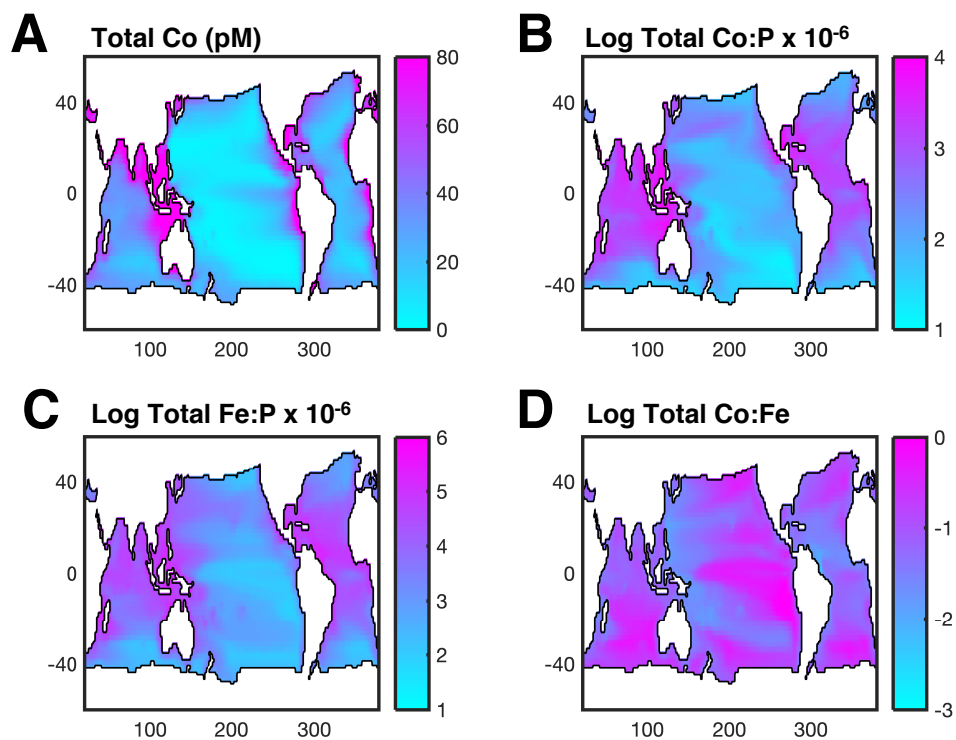


Figure S5. Investigations of surface ocean Co, Fe and P stoichiometry in the PISCES biogeochemical model over the *Prochlorococcus* habitat (defined as waters with temperatures $>12^{\circ}\text{C}$). A) Modelled distribution of total cobalt (sum of dissolved and particulate fields). B) The ratio of total cobalt (panel A) to total phosphorus (the sum of seawater phosphate and particulate fields). C) The ratio of total Fe to total phosphorus. Note that this does not include refractory Fe pools from dust, which are not explicitly modelled here. D) the ratio of total cobalt to total Fe.

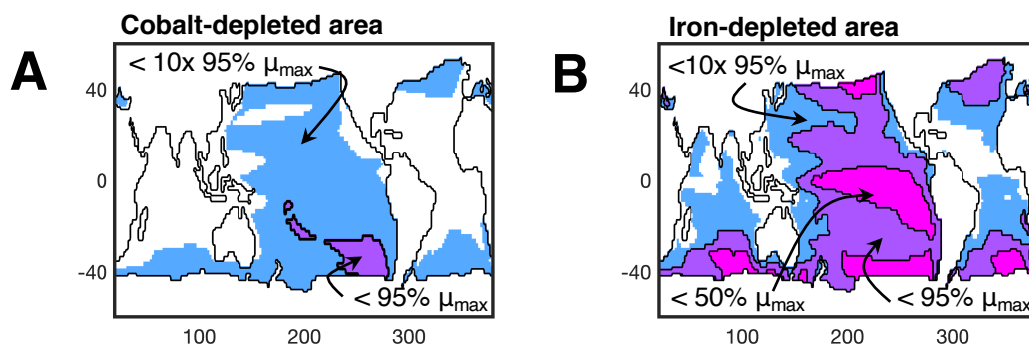


Figure S6. A) Distribution of cobalt poor environments within the PISCES biogeochemical model in the surface ocean. Purple shading indicates surface waters that are depleted in cobalt, having a Co:PO₄ ratio below the 95% μ_{\max} threshold of *Prochlorococcus* MIT9215 (26×10^{-6} , Table S1). Blue shading indicates regions where Co:PO₄ ratios are less than a factor of 10 above the 95% μ_{\max} threshold (i.e. $26 < \text{Co:PO}_4 < 260 \times 10^{-6}$). The value of 260×10^{-6} corresponds to Co:P ratios in zinc-starved *Emiliana huxleyi* (26). B) Distribution of iron poor environments. Purple and blue regions are defined as in A, representing 95% μ_{\max} and 10x 95% μ_{\max} . Pink regions highlight areas with a modelled Fe:PO₄ ratio below a 50% μ_{\max} threshold of *Prochlorococcus* MIT9215.

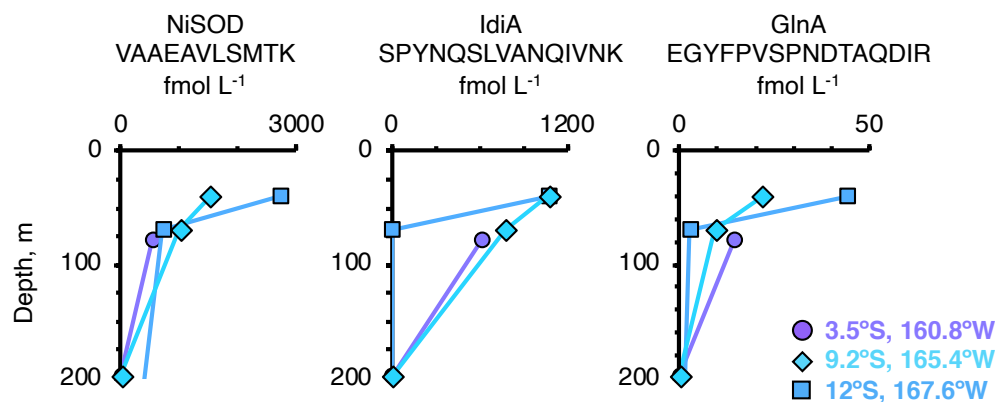


Figure S7. Profiles of *Prochlorococcus*-specific proteins in the South Pacific Gyre from the Metzyme expedition (October 2011). Peptides corresponding to the nickel-dependent superoxide dismutase (NiSOD), the iron deficiency induced protein (IdiA), and Glutamine Synthetase (GlnA) are shown. The abundance of the IdiA protein, which may be an inorganic iron transporter, is indicative of Fe stress (27). These profiles also suggest that *Prochlorococcus* activity is greater near the mixed layer than in the deep chlorophyll maximum layer (75–125 m; Fig. S4). Original data are described by Saito et al. (2014) (15) and can be accessed at <https://www.bco-dmo.org/dataset/646115>.

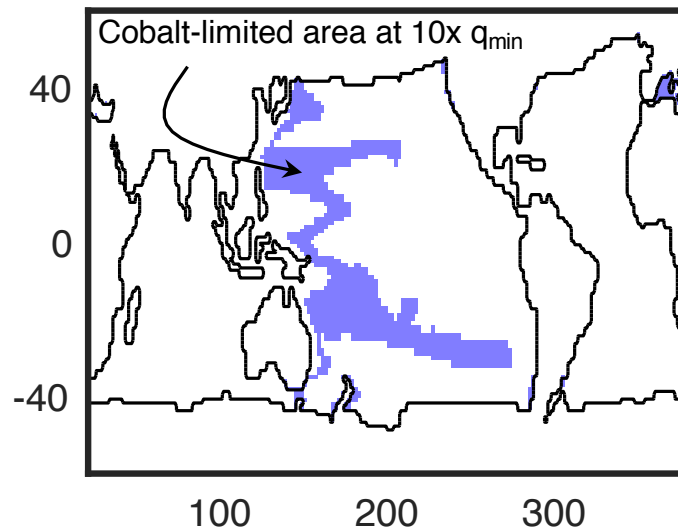


Figure S8. Predicted regions of *Prochlorococcus* cobalt limitation if minimum cobalt requirements were 10-fold higher than measured values, as found in *Emiliana huxleyi* grown in low Zn media. Under these conditions, cobalt limitation is expected to exceed iron and macronutrient limitation for ~12% of surface waters >12°C. The distribution of cobalt depleted waters at this threshold is considerably larger (~55%, Figure S6) but Fe is more strongly depleted in most of that area.

GGATCCATGACACCAGAATTTCTCCGGAGCGTGAGCGAAGTGGGCATTACCCCGAAAACACCAGAATTCCTTCGCGGC
TTTGGCGGCATGGCGAACCCGATTAAAACCTCCTGAATTTCTGCGTGTGGCGAGCCTGCTGGGCAAAAACACCAGAATT
TCTCCGGGTGTATCATACCAAACCGAGCTATCAGACCATTCTGGATGCGGTGACCAAAACTCCTGAATTCCTTCGCG
AAAACGAAATTGAAGATCTGAGCCGCACACCAGAGTTTCTCCGGTTTAGCGCGAACGCGACCTTTCCGCGC
ACTCCTGAATTCCTTCGCGTGTGGCGGGCAGCATTGGCCCCGACCACCAAAAACACCAGAGTTTCTGCGTGC
GGGCCTGGATAGCGCGATTATTGCGCCGAACAAAACCTCCGGAATTCCTGCGTGCCTTTAGGATCTGAGCATT
CAGGATTTTAAAACCCCGAATTCCTTCGCGATTAGCCAGTTTAACTTTCCGCGCACTCCC
GAATTCCTGCGCGTGAGCGATAGCAACATTCAGCTGAGCCTGCTGGATGCGAAAACCCCGAATTTCTCCGGT
GGATCTGAGCACCATGGAAGAAAGCAGCTGGACCGCAGCCTGACCAAAACGCCGAGTTCTCCGT
TTTCTGGAAGTGAACGGCGATTGGATGGCGACCCATCGCACCCCGAATTTCTGCGCGTGGAAGCGGATATT
TCTGCGCGTGGAAGCGGATATTGCGGGCCATGGCCAGGAAGTGCTGATTTCGCACCCCTGAGTTTCTTCGTCT
GTTTACCGGCCATCCGGAAACCCCTGGA AAAACACCAGAGTTTCTGCGTGGCCATCATGAAGCGGAACTGAA
ACCGCTGGCGCAGAGCCATGCGACCAAAACTCCGGAATTCCTGCGTCATCCGGGCGATTTTGGCGCGGAT
GCGCAGGGCGCGATGACCAAAACTCCTGAATTTCTGCGTGCGCTGGAACTGTTTTCGCACCCCTGAGTTTCT
TCGTGAACTGGGCTTTTCAGGGCACTCCTGAATTCCTTCGCGTTACTC
GAG

Figure S9. Plasmid Sequence used for cloning ¹⁵N-labeled peptides for *Prochlorococcus* MIT9215 NrdJ and MetH enzymes. Color scheme: Yellow: Restriction enzymes (5' BamH1, 3' Xho1), Blue: Start/Stop codons, Green: NrdJ peptides, Cyan: MetH peptides, Pink: peptides associated with a *Prochlorococcus* protein of unknown function, Grey: myoglobin, spacer peptides (colorless).

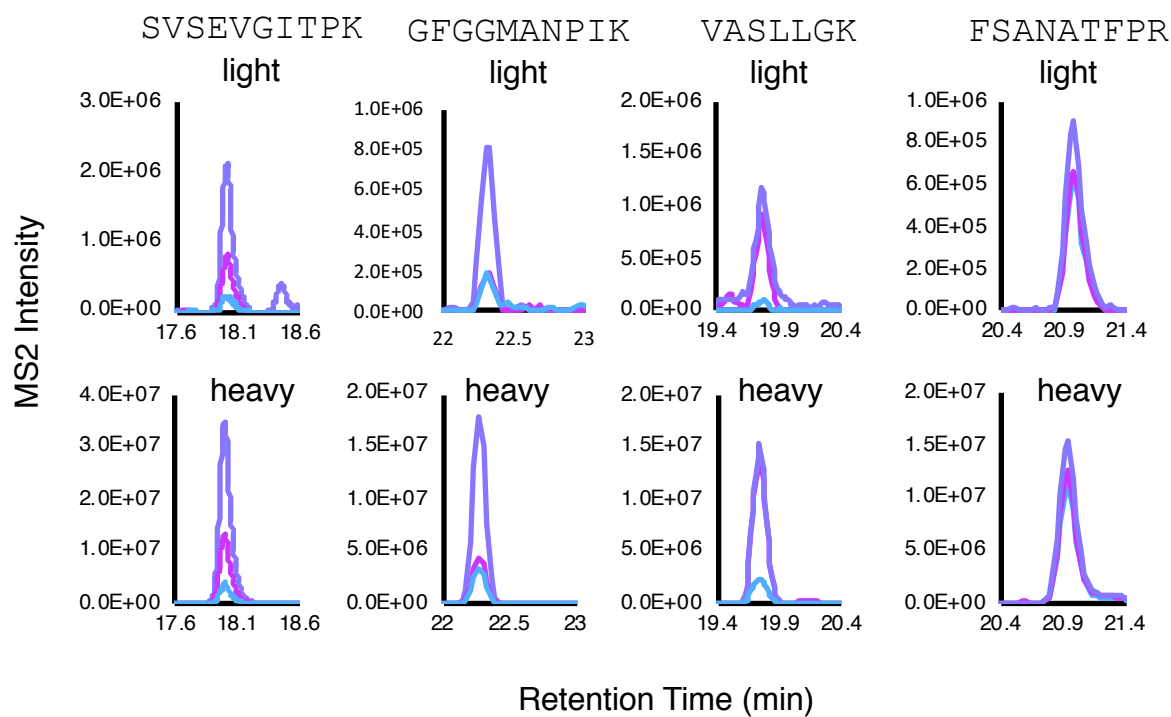


Figure S10. Peptide chromatograms for the ribonucleotide triphosphate reductase from *Prochlorococcus* MIT9215 (NrdJ, 9215_07641). Upper panels show light (unlabeled) peptides deriving from *Prochlorococcus* MIT9215 biomass. Lower panel shows chromatograms for heavy (labeled) peptides. Different lines represent prominent ms^2 fragments. Color coding is consistent between upper and lower panels.

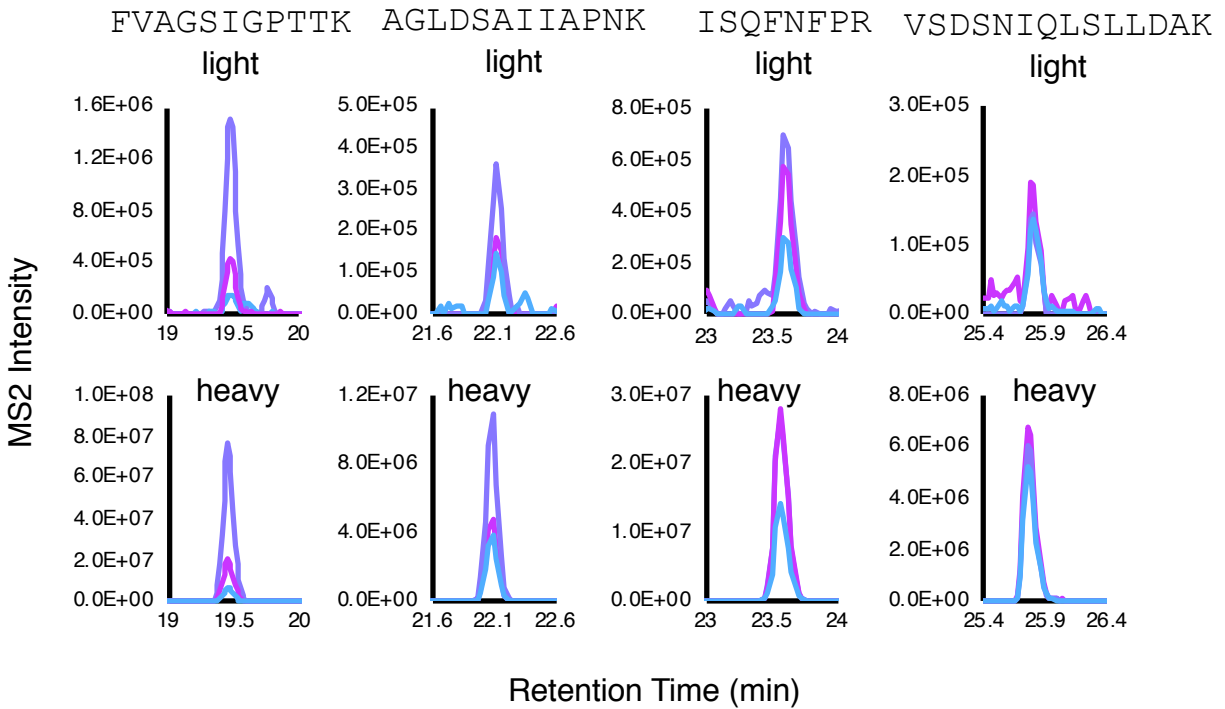


Figure S11. Peptide chromatograms for the methionine synthase from *Prochlorococcus* MIT9215 (MetH, P9215_10151). Upper panels show light (unlabeled) peptides deriving from *Prochlorococcus* MIT9215 biomass. Lower panel shows chromatograms for heavy (labeled) peptides. Different lines represent prominent m/z fragments. Color coding is consistent between upper and lower panels.

3. Supplemental Tables

Table S1. Cobalt and iron limitation thresholds of *Prochlorococcus* MIT9215. Values of q_{\min} are derived from least-squares regressions to the Droop Equation (Eq. 1 in main text) using the data in Table S2. Separate regressions were derived for cell quota (atom cell⁻¹), metal:P and metal:C ratios (resulting in different R²). Empirical metal use efficiencies, in mol C day⁻¹ (mol metal)⁻¹, are calculated as the maximum ratio of growth rate (μ) over the metal:C ratio.

	Co cell ⁻¹	Co:P	Co:C	Fe cell ⁻¹	Fe:P	Fe:C
q_{\min}	14.8 ±	1.34 ±	6.05 ± 0.49	1550 ±	0.26 ± 0.04	0.81 ± 0.10
($\mu = 0$)	1.3	0.09 x 10 ⁻⁶	x 10 ⁻⁹	170	x 10 ⁻³	x 10 ⁻⁶
20x q_{\min}	296	26.7 ±	121 ± 9.83 x	31,000 ±	5.17 ± 0.79	16.2 ± 2.05
($\mu = 0.95 \mu_{\max}$)	± 26	1.83 x 10 ⁻⁶	10 ⁻⁹	3400	x 10 ⁻³	x 10 ⁻⁶
R ²	0.955	0.972	0.961	0.956	0.916	0.943
Use efficiency (empirical)**			1.55 x 10 ⁷			1.52 x 10 ⁵

* μ_{\max} Fe = 0.57; μ_{\max} Co = 0.55

** = max(μ /metal:C).

Table S2. Contents of *Prochlorococcus* MIT9215 in unwashed cells under cobalt and iron limitation. Bolded values are used to calculate empirical metal use efficiencies in Table S1. Metal:C ratios are calculated assuming a C quota of $1.85 \pm 0.23 \times 10^9$ C atoms cell⁻¹ and a P:C ratio of 325 ± 74 mol:mol (the two approaches are averaged).

[Co] total nM	[Co ²⁺] pM	[Fe] total nM	[Fe ²⁺] pM	μ day ⁻¹	σ	Co atoms cell ⁻¹	Co:C ratio x10 ⁻⁹	σ	Fe atoms cell ⁻¹	Fe:C ratio x10 ⁻⁶	σ	P atoms cell ⁻¹	σ
10.01	15.50	12	134.7	0.549	0.042	779.9	321	157.8	51307	21.1	7.0	1.08E7	2.22E6
3.01	4.66	12	134.7	0.548	0.039	236.4	103	47.3	46202	20.1	6.7	9.25E6	1.87E6
1.01	1.56	12	134.7	0.429	0.048	72.2	39.8	14.6	54760	22.6	7.5	1.07E7	2.17E6
0.61	0.95	12	134.7	0.329	0.021	54.0	21.2	10.8	79901	31.4	10.3	1.25E7	2.51E6
0.31	0.48	12	134.7	0.086	0.012	16.7	6.84	7.0	166841	68.2	27.6	1.15E7	4.14E6
0.11	0.17	12	134.7	0.026	0.018								
5.01	7.76	10.3	115.7	0.561	0.018	341.0	147	68.8	38258	16.4	5.4	9.61E6	1.92E6
5.01	7.76	3.3	37.1	0.526	0.019	264.6	132	53.1	21283	10.6	3.5	6.70E6	1.34E6
5.01	7.76	1.3	14.6	0.477	0.036	240.4	127	48.1	12568	6.66	2.19	5.91E6	1.18E6
5.01	7.76	0.6	6.7	0.402	0.025	272.8	141	56.0	5108	2.64	0.91	6.21E6	1.38E6
5.01	7.76	0.4	4.5	0.234	0.055								

Table S3. Iron Use efficiency calculations for *Prochlorococcus*

Quantity		Units	Reference, Derivation
Iron atoms in Photosynthetic chain	20 (23*)	Atoms per photosynthetic complex	Raven 1990 (28)
Turnover time of PSII	250	Electrons per s	Raven 1988 (29)
Electrons per CO ₂ fixed	4	Electrons	C(+4)O ₂ → C(0)H ₂ O
Ratio CO ₂ fixed per C biomass	1.333	Mol : mol	Raven 1988 (29)
Iron Use efficiency, photosynthesis (24 hour light)	0.427 (0.491*)	Mol Fe per (mol C per s)	= 1.333 x 4 x 20 / 250
Iron Use efficiency, photosynthesis (14:10)	0.731 (0.841*)	Mol Fe per (mol C per s)	= 0.427 x 24 / 14
Iron atoms in respiration	42	Atoms per respiratory complex	Raven 1988 (29)
Turnover time respiratory cytochrome C oxidase	250	Electrons per s	Raven 1988 (29)
Iron Use efficiency, respiration	0.224	Mol Fe per (mol C per s)	= (1.333-1) x 4 x 42 / 250
Total Iron use efficiency	0.955 (1.065*)	Mol Fe per (mol C per s)	= 0.731 + 0.224
	9.04 x 10 ⁴ (8.11 x 10 ⁴ *)	Mol C per day per mol Fe	= 86400 / 0.955
C per cell	1.85 x 10 ⁹		Martiny et al. 2016 (8)
Growth Rate (arbitrary)	0.4	Per day	
Fe quota, predicted	8200 (9140*)	Fe Atoms Per cell	= 0.4 x 1.85 x 10 ⁹ / 9.04 x 10 ⁴
Fe quota, measured	5108 ± 1140	Fe Atoms Per cell	Table S2

*including Fe use in Ferredoxin and Cytochrome C (versus substitution by Flavodoxin and Plastocyanin); assumes equimolar photosynthetic stoichiometry (i.e. PSI:PSII = 1)

Table S4. Cobalt Use Efficiency calculations for *Prochlorococcus*

Quantity		Units	Reference or derivation
Co:NrdJ stoichiometry	1	Mol Co : mol NrdJ	Sintchak et al. 2002 (30)
NrdJ Turnover time	2	Bases Per second	Licht et al. 1999 (13)
NrdJ output, daily	1.73×10^5	Bases per day per NrdJ	= $2 \times 60 \times 60 \times 24$
Genome size	3.4×10^6	dNTP bases*	Kettler et al. 2007 (31)
NrdJ demand	20.1	Copies NrdJ per cell per day	= $3.4 \times 10^6 / 1.7 \times 10^5$
Co demand, nrdJ	20.1	Co per cell per day	
Co:MetH stoichiometry	1	Mol Co:mol MetH	Drennan et al. 1994 (32)
MetH turnover time	18	Methionine molecules per second	Banerjee et al. 1990 (33)
MetH output, daily	1.6×10^6	Methionine molecules per day	= $18 \times 60 \times 60 \times 24$
Maximum methionine molecules per cell	1.2×10^7	Sulfur atoms per cell	Assuming P:S ratio ~ 1 Heldal et al. 2003 (34)
Methionine demand	7.7	Copies met H per cell per day	= $1.2 \times 10^7 / 1.6 \times 10^6$
Co demand, methH	7.7	Co per cell per day	
C per cell	1.85×10^9	Atoms per cell	Martiny et al. 2016 (8)
Co Use efficiency, calculated	6.6×10^7	Mol C per day per mol Co	= $1.85 \times 10^9 / (20.1 + 7.7)$
Co Use efficiency, empirical	1.55×10^7	Mol C per day per mol Co	Table S1
Growth Rate (μ_{max})	0.20 (0.6)	Per day	Table S2
NrdJ quota, predicted	4.0 (11.8)	Copies per cell	= 0.2×20.1
NrdJ quota, measured	15 ± 2	Copies per cell	
MetH quota predicted	1.5 (4.8)	Copies per cell	= 0.2×7.7
MetH quota measured	7 ± 2	Copies per cell	
Co quota, predicted	5.5 (16.6)	Atoms per cell	= $4 + 1.5$
Co quota, measured	65 ± 8	Atoms per cell	

*1.7 million base pairs

Table S5. Peptide and DNA sequences of used in plasmid construction.

Ribonucleotide reductase NrdJ	
SVSEVGITPK	AGCGTGAGCGAAGTGGGCATTACCCCGAAA
GFGGMANPIK	GGCTTTGGCGGCATGGCGAACCCGATTAAA
VASLLGK	GTGGCGAGCCTGCTGGGCAAA
VYHTKPSYQTILDAVTK	GTGTATCATACCAAACCGAGCTATCAGACCATTCTGGATGCGGTGACCAAA
SLLTGAAPGWHPK	AGCCTGCTGACCGGCGCGGCGCCGGCTGGCATCCGCCGAAA
ENEIEDLSR	GAAAACGAAATTGAAGATCTGAGCCGC
FSANATFPR	TTTAGCGCGAACGCGACCTTTCCGCGC
YDVGELSEAGPAGCDSK	TATGATGTGGGCGAACTGAGCGAAGCGGGCCCGCGGGCTGCGATAGCGATAAA

Methionine synthase MetH	
ELEGCNENLVLSSPNVVER	GAAGTGAAGGCTGCAACGAAAACCTGGTGTCTGAGCAGCCCGAACGTGGTGGAAACGC
FVAGSIGPTTK	TTTGTGGCGGGCAGCATTGGCCCGACCACCAAA
AGLDSAI IAPNK	GCGGGCCTGGATAGCGCGATTATTGCGCCGAACAAA
AFQDLSIQDFK	GCGTTTCAGGATCTGAGCATTTCAGGATTTTAAA
INLNSIFLDEC IK	ATTAACCTGAACAGCATTTTTCTGGATGAATGCATTAAA
ISQFNFR	ATTAGCCAGTTTAACTTTCCGCGC
YSFGYPACPK	TATAGCTTTGGCTATCCGCGGTGCCCGAAA
VSDSNIQLSLLDAK	GTGAGCGATAGCAACATTTCAGCTGAGCCTGCTGGATGCGAAA

Myoglobin	
VEADIAGHGQEV LIR	GTGGAAGCGGATATGCGGGCCATGGCCAGGAAGTGTGCTGATTCGC
LFTGHPETLEK	CTGTTTACCGCCATCCGGAACCTGGAAAAA
GHHEAELKPLAQSHATK	GGCCATCATGAAGCGGAACTGAAACCGCTGGCGCAGAGCCATGCGACCAAA
HPGDFGADAQGAMTK	CATCCGGGCGATTTTGGCGCGGATGCGCAGGGCGCGATGACCAAA
ALELFR	GCGCTGGAAGTGTTCGC
ELGFQG	GAAGTGGGCTTTCAGGGC

Table S6. Calibration of ^{15}N labeled myoglobin peptides to 100 fmol ^{14}N myoglobin peptides. Duplicate injections shown.

Peptide Sequence	Injection Number	Peptide Peak Found Ratio	Peptide Retention Time (minutes)	Ratio To Standard
VEADIAGHGQEVLR	1	1	21.83	2.4049
VEADIAGHGQEVLR	2	1	21.68	2.3136
LFTGHPETLEK	1	1	19.71	2.6456
LFTGHPETLEK	2	1	19.47	2.7566
GHHEAELKPLAQSHATK	1	1	15.33	2.5027
GHHEAELKPLAQSHATK	2	1	14.87	2.1853
ALELFR	1	1	25.98	2.7962
ALELFR	2	0.94	25.92	2.9433
HPGDFGADAQGAMTK	1	1	18.9	4.1635
HPGDFGADAQGAMTK	2	1	18.6	4.1598
Median				2.701

Table S7. Quantitation of MetH and NrdJ peptides in large volume *Prochlorococcus* cultures and comparison to cobalt quotas measured by ICP-MS. Measurements of strongly limited cells ($\mu = 0.2 \text{ day}^{-1}$) are shown in Figure 1C.

Growth Rate (day ⁻¹)	Abundance (cells ml ⁻¹)	Cobalt (atoms cell ⁻¹)	Ribonucleotide reductase NrdJ (copies per cell \pm 1SD)									
			SVSEVGITPK		GFGGMANPIK		VASLLGK		FSANATFPR		Mean	\pm
0.2	5.7E+07	98	13.5	0.1	12.6	0.2	15.4	0.1	14.3	0.2	13.9	1.2
0.2	6.9E+07	86	15.6	0.3	12.5	0.2	17.8	1.0	14.3	0.3	15.0	2.2
0.2	1.0E+08	72	11.6	0.0	13.5	0.2	15.2	1.7	12.3	0.1	13.2	1.6
0.32	4.6E+07	70	11.3	0.1	8.7	0.4	12.0	0.1	11.3	0.3	10.8	1.5
0.32	9.7E+07	65	10.8	0.3	9.4	0.1	12.6	0.4	10.4	0.4	10.8	1.4
0.32	1.3E+08	62	15.1	0.2	12.5	0.4	16.2	0.6	14.5	0.6	14.6	1.6

Growth Rate (day ⁻¹)	Abundance (cells ml ⁻¹)	Cobalt (atoms cell ⁻¹)	Methionine Synthase Meth (copies per cell \pm 1SD)									
			FVAGSIGPTTK		AGLDSAIAPNK		ISQFNFPK		VSDSNIQLSLDAK		Mean	\pm
0.2	5.7E+07	98	4.2	0.2	7.8	0.1	5.0	0.0	5.4	0.1	5.6	1.6
0.2	6.9E+07	86	5.7	0.4	9.5	0.3	6.7	0.7	7.3	0.8	7.3	1.6
0.2	1.0E+08	72	4.3	0.4	6.9	0.1	4.7	0.5	5.6	0.2	5.4	1.1
0.32	4.6E+07	70	5.6	0.1	8.9	0.1	6.1	0.0	7.4	0.4	7.0	1.5
0.32	9.7E+07	65	5.2	0.2	9.1	1.0	5.7	0.3	7.0	0.6	6.8	1.8
0.32	1.3E+08	62	8.2	0.5	14.8	0.3	9.1	0.2	12.4	0.4	11.2	3.0

Table S8. Spectral counting of *Prochlorococcus* MIT9215 proteomes from the cobalt gradient experiment. Only proteins identified in all cobalt-limited (0.6 and 1 nM) or in all cobalt-replete (10 and 3 nM) samples are shown. Fisher exact tests compare Cobalt Replete and Cobalt Limited groups.

<i>Identified proteins n = 484</i> <i>Significant proteins n = 56 (Fischer exact p<0.01)</i>	Cobalt Replete				Cobalt Limited			
	10 nM		3 nM		1 nM		600 pM	
	A	B	A	B	A	B	A	B
<i>Upregulated proteins (n=20, Fisher exact p<0.01)</i>								
50S ribosomal protein L20	3	8	6	2	15	33	4	13
Photosystem II manganese-stabilizing protein	20	48	34	39	60	88	73	62
60 kDa chaperonin 2	113	142	73	66	172	157	134	148
50S ribosomal protein L2	71	111	85	80	176	169	119	136
Helix-hairpin-helix DNA-binding protein containing motif class 1	5	2	4	0	21	16	11	3
Thioredoxin	36	60	38	46	69	85	79	77
50S ribosomal protein L7/L12	25	28	34	29	56	50	58	51
ATP synthase subunit b	7	13	16	13	19	35	29	26
Photosystem I protein PsuD	37	40	24	21	81	70	44	24
Putative Branched-chain amino acid aminotransferase	24	20	12	14	37	39	33	31
Ribulose biphosphate carboxylase, small chain	150	120	99	129	113	161	95	131
50S ribosomal protein L16	17	12	6	10	29	32	18	17
Ferritin	15	12	13	9	32	17	35	18
Histone-like DNA-binding protein	62	137	74	130	121	178	143	153
50S ribosomal protein L19	45	67	41	24	88	74	75	47
50S ribosomal protein L15	23	16	15	23	32	37	28	42
Single-stranded DNA-binding protein	7	11	0	14	12	22	13	23
Nucleoside diphosphate kinase	18	12	10	0	25	18	24	14
Putative DNA-directed RNA polymerase (omega chain)	19	47	24	35	49	62	46	47
Protein GrpE	30	41	46	21	66	59	62	32
<i>Downregulated proteins (n=14, Fisher exact p<0.01)</i>								
D-fructose 1,6-bisphosphatase class 2/sedoheptulose 1,7-bisphosphatase	42	110	24	14	65	33	40	16
Uncharacterized protein	75	52	77	64	63	48	63	55
Ribulose biphosphate carboxylase large chain	22	44	16	16	28	12	2	8
Transketolase	75	59	45	44	30	45	6	3
30S ribosomal protein S16	23	48	28	46	32	51	12	7
30S ribosomal protein S4	13	25	18	12	13	6	4	0
ATP synthase gamma chain	17	19	10	11	15	7	3	0
Putative nicotinamide nucleotide transhydrogenase, subunit alpha 1 (A1)	9	7	3	4	3	2	0	0
ATP synthase subunit beta	100	121	78	89	104	124	64	70
30S ribosomal protein S13	24	14	10	8	10	9	8	6
30S ribosomal protein S3	6	5	5	2	5	0	0	0
50S ribosomal protein L11	10	21	6	11	11	5	10	3
30S ribosomal protein S10	13	11	5	13	9	15	2	0
Thioredoxin peroxidase	16	14	0	5	7	5	3	6
<i>Not significantly regulated proteins (n=87, p>0.01)</i>								
Ferredoxin-NADP oxidoreductase (FNR)	36	39	19	25	31	41	28	8
50S ribosomal protein L17	25	29	24	21	51	43	37	27

<i>Not significantly regulated proteins (continued)</i>	10 nM		3 nM		1 nM		600 pM	
	A	B	A	B	A	B	A	B
ABC-type Fe ³⁺ transport system, periplasmic component	21	25	12	16	42	35	22	24
50S ribosomal protein L18	15	53	36	31	49	73	40	45
50S ribosomal protein L35	9	7	8	13	15	17	15	22
Uncharacterized protein	8	8	10	7	11	21	24	7
50S ribosomal protein L27	8	7	8	5	8	6	4	0
Protoporphyrin IX Magnesium chelatase, ChI subunit	22	10	4	3	16	6	7	0
10 kDa chaperonin	9	13	7	6	19	19	19	7
ATP synthase subunit alpha	65	67	36	42	67	73	36	39
Possible cAMP phosphodiesterase class-II	6	6	0	0	9	9	7	3
50S ribosomal protein L23	8	13	9	3	21	17	10	12
30S ribosomal protein S7	29	39	33	33	53	49	18	11
Elongation factor Tu	99	133	52	100	74	91	111	137
Triosephosphate isomerase	21	29	20	2	31	30	0	4
Uncharacterized protein	18	19	23	24	26	41	39	23
NifU-like protein	4	8	7	2	7	8	14	10
Signal peptide peptidase SppA (Protease IV)	10	3	2	4	16	8	9	4
Photosystem I iron-sulfur center	17	19	20	23	46	23	24	28
Chaperone protein DnaK	34	37	26	9	41	26	27	11
Ribosomal protein S1	24	28	17	11	26	23	18	10
Carboxysome shell protein CsoS2	37	41	49	29	73	47	62	39
Putative nickel-containing superoxide dismutase (NISOD)	10	14	6	8	9	6	11	7
Glutamate-1-semialdehyde 2,1-aminomutase	10	12	5	5	11	7	4	5
Pyridoxine 5'-phosphate synthase	9	6	11	9	15	10	15	17
50S ribosomal protein L13	18	18	11	7	24	23	15	20
Ornithine carbamoyltransferase, catabolic	8	10	15	2	14	18	15	9
Dihydrolipoyl dehydrogenase	17	11	8	3	15	13	6	2
Enolase	25	22	10	6	39	20	16	18
Uncharacterized protein	2	5	6	3	6	4	0	2
Elongation factor P	12	11	15	4	16	10	12	2
Glutamine synthetase	58	142	56	76	114	101	126	94
Flavodoxin	6	16	4	15	11	20	16	15
Delta-aminolevulinic acid dehydratase	8	7	0	5	8	14	2	8
Photosystem I PsaF protein (Subunit III)	20	12	7	3	25	16	0	0
50S ribosomal protein L1	12	9	8	11	15	9	10	5
50S ribosomal protein L24	9	0	2	0	7	7	4	2
Uncharacterized protein	29	13	6	5	24	14	10	6
Uncharacterized protein	14	11	7	12	19	18	14	13
Carboxysome shell protein CsoS1	243	329	142	243	326	307	249	245
Uncharacterized protein	14	15	6	6	20	16	16	8
Polyribonucleotide nucleotidyltransferase	20	13	8	9	14	15	11	11
Fructose-bisphosphate aldolase	20	31	20	15	50	29	7	6
50S ribosomal protein L4	72	212	107	97	193	153	129	92
Uncharacterized protein	20	36	25	20	32	24	31	24
DNA-directed RNA polymerase subunit beta'	24	14	5	0	18	15	6	5
S-adenosylmethionine synthase	15	23	13	10	25	23	10	7
50S ribosomal protein L32	9	7	8	9	7	4	14	8
50S ribosomal protein L14	21	14	15	11	25	13	20	7
Cell division protein FtsZ	32	49	24	18	52	41	38	32
50S ribosomal protein L3	20	22	8	7	26	26	16	11
30S ribosomal protein S5	17	12	6	10	20	24	3	0
Soluble hydrogenase small subunit	9	5	0	5	6	8	7	8
50S ribosomal protein L9	15	19	8	18	21	24	17	20
50S ribosomal protein L29	4	11	2	3	8	9	8	5
50S ribosomal protein L6	33	26	27	21	42	30	22	26

<i>Not significantly regulated proteins (continued)</i>	10 nM		3 nM		1 nM		600 pM	
	A	B	A	B	A	B	A	B
Ribosome-recycling factor	7	0	3	4	9	2	6	5
60 kDa chaperonin 1	31	18	8	8	32	19	9	11
Putative IMP dehydrogenase	49	60	42	70	71	92	51	41
30S ribosomal protein S15	10	15	9	3	19	28	5	0
30S ribosomal protein S6	17	17	28	9	36	19	23	0
Two-component response regulator	20	14	11	11	24	17	21	14
3-oxoacyl-[acyl-carrier-protein] synthase 2	9	8	6	6	12	8	6	4
Two-component response regulator	8	7	2	3	10	5	3	2
ATP-dependent zinc metalloprotease FtsH	7	11	6	3	15	12	5	6
50S ribosomal protein L28	9	6	4	3	15	11	2	3
Photosystem II lipoprotein Psb27	11	5	7	4	12	7	8	2
ATP synthase subunit b'	14	8	8	3	15	5	9	7
Light-harvesting complex protein	12	10	4	6	11	13	11	8
Putative GTP cyclohydrolase I	11	9	7	9	15	14	8	11
Photosystem II D2 protein	5	5	4	4	6	13	0	0
Phosphate-binding protein	11	16	16	11	23	15	18	14
30S ribosomal protein S14	22	42	14	12	37	29	23	16
30S ribosomal protein S18	8	7	9	13	16	15	13	5
ATP-dependent zinc metalloprotease FtsH	14	8	7	7	15	15	7	10
Actin-like ATPase involved in cell morphogenesis	15	21	10	16	11	20	18	30
Photosystem II reaction center Psb28 protein	15	29	17	40	29	35	32	30
Biotin carboxyl carrier protein	9	16	6	11	11	20	9	9
Glyceraldehyde-3-phosphate dehydrogenase	14	10	3	4	17	9	7	7
Uncharacterized protein	11	8	9	6	11	14	7	8
50S ribosomal protein L5	17	19	17	14	23	25	13	19
Peptidyl-prolyl cis-trans isomerase	36	41	26	25	38	54	35	31
Putative potassium channel, VIC family	6	7	4	0	6	3	9	4
DNA-directed RNA polymerase subunit alpha	66	62	33	53	85	61	70	46
Pentapeptide repeat-containing proteins	20	24	6	11	16	33	16	10
Cysteine synthase	5	9	2	0	5	5	4	5
DNA-directed RNA polymerase subunit beta	12	9	6	0	11	8	8	6